The Thesis Committee for Christopher Ainslie van der Hoeven
Certifies that this is the approved version of the following thesis:

Three Technical Challenges Facing Advanced Fuel Cycle Closure

APPROVED BY
SUPERVISING COMMITTEE:

Supervisor:

Erich Schneider

Steven Biegalski

Three Technical Challenges Facing Advanced Fuel Cycle Closure

by

Christopher Ainslie van der Hoeven, B.S.

Thesis

Presented to the Faculty of the Graduate School of

The University of Texas at Austin

in Partial Fulfillment

of the Requirements

for the Degree of

Masters of Science in Engineering

The University of Texas at Austin

December, 2009

Acknowledgements

I would like to thank Dr. Erich Schneider for his mentorship and help throughout my graduate studies. I would also like to thank Dr. Swadesh M. Mahajan, Dr. Mike Kotschenreuther, and Dr. Prashant Valanju of the Institute for Fusion Studies. Finally, I would like to thank my family and friends who have helped make this all worthwhile.

4 December 2009

Abstract

Three Technical Challenges Facing Advanced Fuel Cycle Closure

Christopher Ainslie van der Hoeven, MSE

The University of Texas at Austin, 2009

Supervisor: Erich Schneider, Ph. D.

Many technical hurdles remain to be overcome before an advanced fuel cycle in which minor actinides from spent nuclear fuel are used to generate power. Three such issues were addressed: criticality safety of minor actinides as compared to currently used fissile isotopes; accuracy of evaluated nuclear data for selected minor actinide high energy fission cross-sections; and the preliminary design optimization of a minor actinide burning/breeding fission blanket in a fission fusion hybrid reactor concept. For minor actinide compositions found in spent fuel, current safety measures for actinide solutions were found to be adequate, though concerns may remain for unmoderated transuranic materials. Additionally, computational results indicated a 5-10% error in the fission cross-section of some minor actinides above the fast fission threshold. Finally, a relatively tall annular fission blanket was found to be the most ideal configuration for the UT fission-fusion hybrid reactor concept, satisfying criticality and power output criteria.

Table of Contents

List of Tables

List of Figures

CHAPTER 1: INTRODUCTION

Many technical hurdles remain to be overcome on the back end for fuel cycles involving reprocessing of spent fuel and advanced fast spectrum reactor concepts. The once-through fuel cycle currently in place in the U.S. has provided electricity for nearly 60 years, and has been both economical and safe. However, it is not without drawbacks, notably the time scale associated with the hazard presented by spent nuclear fuel. Once burned fuel has been ejected from a reactor it can take tens of thousands of years for it to decay back to the levels of radioactivity present in natural uranium ore. The long tail of this decay is dominated by the radioactivity of high Z minor actinides. If these minor actinides were to be separated from the spent fuel and fissioned themselves, the resulting radioactive products would present a hazard with a time scale of centuries rather than millennia (Martinez, 2000). This decrease in turn could both improve the economics of nuclear power as well as improve the public perception of the industry. However, such a fuel cycle would need to overcome many technical challenges, some of which this thesis will seek to address.

The first of these issues is that of criticality safety for advanced reprocessing facilities. Reprocessing techniques currently used involve the dissolution of spent fuel in nitric acid, separation of uranium and plutonium, and disposal of the remaining high level waste containing minor actinides and fission products (NEI, 2006). Further separation of the minor actinides would require the implementation of safety measures to ensure criticality accidents do not occur. These safety protocols may differ substantially from those for uranium and plutonium, as most of the minor actinides exhibit threshold fission behavior: below neutron energies of about 100 keV they will not fission. Therefore, unlike uranium and plutonium which have lower minimum critical masses when in solution, reprocessing streams containing solely minor actinides would have a lower multiplication factor when dilute, and conversely a higher multiplication factor when concentrated. For the purposes of this research, a standard benchmark of a multiplying solution was modeled using MCNPX, and plots of concentration vs. minimum critical

mass were generated for the constituent minor actinides of varying burn up spent fuel. These plots provide a tool for criticality comparison between the spent fuel minor actinides and standard fuel isotopes such as ^{235}U, and can in turn be used by designers to scale processes involving these spent fuel compositions.

However, the MCNPX modeling used to generate the plots mentioned above, and any modeling using current evaluated nuclear data does so with the assumption that the nuclear data is accurate. For many elements and common isotopes the reaction cross-section data is extremely accurate, and more than adequate for safety and design. The accuracy of data for other less studied isotopes, such as the minor actinides, is more suspect (Mengoni, *et al*, 2008). As the minor actinides only exist in large quantities in spent fuel it is difficult and costly to experimentally verify their cross-section data; interaction models are used extensively to help fill in gaps in the experimental data. Using experimental results from the Japan Atomic Energy Agency's (JAEA) unique Fast Critical Assembly (FCA) facility, one of very few experimental data sets to address these isotopes, this research attempted to quantify possible inaccuracy in the fast fission cross-section data of several important minor actinides; ^{241}Am, ^{243}Am, ^{244}Cm, ^{237}Np, ^{238}Pu, and ^{242}Pu. Furthermore, an attempt was made to determine a correction factor for specific energy regions in the cross-section data for each actinide, the application of which would most greatly reduce the error between the reported experimental data and the computational results. This correction factor is intended to guide further research to the energy regions in which errors in the cross-section data are evident.

Finally, assuming minor actinides as a fuel form, an advanced reactor concept would be required to utilize that fuel. Specifically, a fast spectrum system would be necessary to overcome the fission threshold of many of the actinides. Many Fast Burner Reactor concepts have been proposed and designed over the years, and a few have been constructed and operated successfully. One concept first proposed over 50 years ago is that of a hybrid fusion-fission system. Such a system would utilize the fast neutrons produced from fusion to drive the fission reactions in a subcritical fission blanket. Thanks to its extremely hard spectrum the FFH could burn some of the most difficult to dispose

of actinides, while thanks to its subcritical fission region the system may have a greater margin of safe operation than other systems such as sodium cooled fast reactors. Additionally, the FFH could be used as an effective breeder should the breeding of fissile material become economically viable. Currently a hybrid system based on a compact fusion neutron source is being design by faculty in the UT physics department. The final section of this thesis details the MCNP modeling of the design progression of the fission blanket of that system, varying geometry and structural materials. Additionally, preliminary calculations of viability of the proposed system for breeding with thorium are also included.

These projects seek to address issues unique to fuel cycle concepts utilizing minor actinides. Design of both advanced reactors to burn minor actinides as fuel and the facilities necessary to reprocess and fabricate that fuel will require a sound knowledge base for these species, including accurate cross-section and criticality data. Experimental data for many of the minor actinides is sparse, and analysis as presented herein had not previously been completed.

In summary, the three goals of this work are to examine criticality safety issues for reprocessing streams containing minor actinides, determine energy regions containing potential inaccuracies in the fission cross-sections of several key minor actinides, and present an initial design optimization completed for the fission blanket of a proposed fission-fusion hybrid system.

CHAPTER 2: SPENT FUEL MINOR ACTINIDE CRITICALITY SAFETY

The original focus of this research is on criticality safety, particularly addressing criticality issues that might be encountered due to spent fuel reprocessing in an advanced closed fuel cycle. Past reprocessing techniques, such as PUREX, call for the separated streams of uranium and plutonium isotopes from SNF to be recycled in MOX fuel elements, along with a stream of minor actinides, such as isotopes of neptunium, americium, and curium, for long term disposal. The presence of a pure plutonium stream in this separation scheme is viewed as an unacceptable proliferation risk by some, and therefore newer reprocessing schemes, such as the UREX suite of techniques, does not separate the plutonium completely from the minor actinides (Laidler, *et al,* 2001). Additionally, future reprocessing plans may call for multiple fuel types to be derived from spent fuel, for example, MOX fuel to be burned in thermal spectrum reactors and minor actinide only fuel to be burned in advanced fast spectrum reactors. Both of these scenarios would call for reprocessing chemistry involving solutions of minor actinides which, depending on composition, concentration, and geometry could present criticality safety issues.

Additionally, it should be noted that analyzing these solutions of minor actinides is predominantly accomplished computationally, due to the safety and cost concerns of experimental work with spent fuel minor actinides. Therefore, as they are the key to accurate computational results, correct cross-section data for the minor actinides is critical to such research.

CRITICALITY BENCHMARK

One basis for criticality safety study is benchmark criticality tests, in which critical systems are constructed and very accurately measured with respect to composition and geometry. Standard benchmarks include uranium and plutonium metals or solutions, reflected by various materials and in various geometries, and of varying enrichment. The resulting benchmark data is maintained by the NEA Nuclear Science

committee in its International Handbook of Evaluated Criticality Safety Benchmark Experiments. Unfortunately, very few benchmark experiments have been performed for the minor actinides, with the exception of a series of metal sphere tests for ^{237}Np.

As there was a lack of minor actinide benchmark tests available a mixed plutonium/uranium benchmark was selected instead. The experiment chosen was titled, "Criticality Experiments with Mixed Plutonium and Uranium Nitrate Solution at a Plutonium Fraction of 0.2 and 0.5 in Large Cylindrical Geometry," and was conducted by researchers at Lawrence Livermore National Laboratory in September of 2000, and was reviewed by Oak Ridge National Lab (Pohl, *et al*, 2000). The experimental set-up consisted of a stainless steel cylinder containing the plutonium/uranium nitrate solution surrounded by a water reflector, as shown on the right hand side of figure 1.

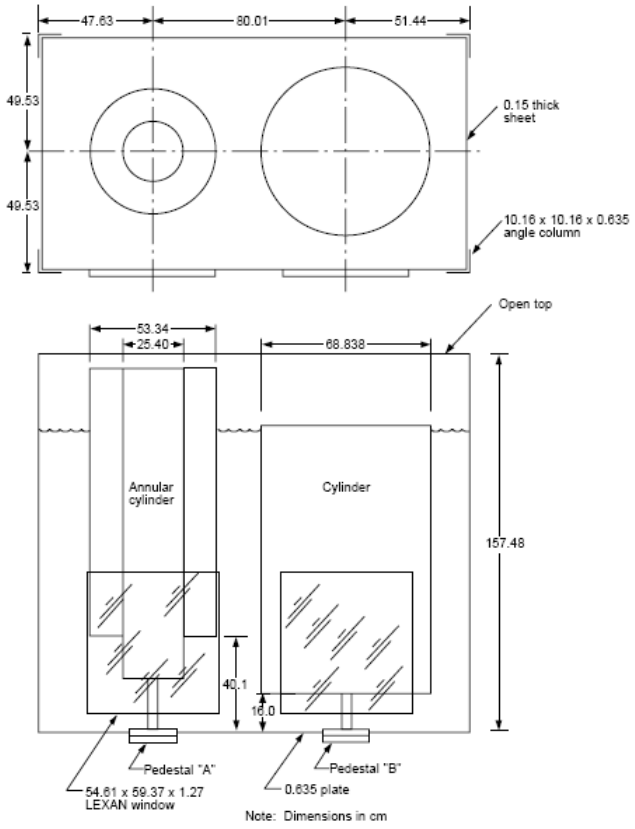

Figure 1. Schematic of Experimental Vessel Arrangement, G. R. Smolen et al., "Criticality Data and Validation Studies of Plutonium-Uranium Nitrate"

For the case studied, a critical height of solution within the cylinder of 76.80 cm was reported, with a MCNP calculated multiplication factor of 1.0082 ± 0.0002. For the results provided, MCNP version 4a was run with ENDF/B-V cross-section library for all materials except for natural gadolinium for which the cross sections were extracted from the ENDL-85 library. These results were duplicated, calculating a multiplication factor of 1.00819 using MCNPX and the same data libraries. The MCNPX geometry used is shown in figure 2, where yellow denotes stainless steel and purple the actinide solution. From this preliminary result, it appears the nuclear data for uranium and plutonium is accurate to within the error of this experiment.

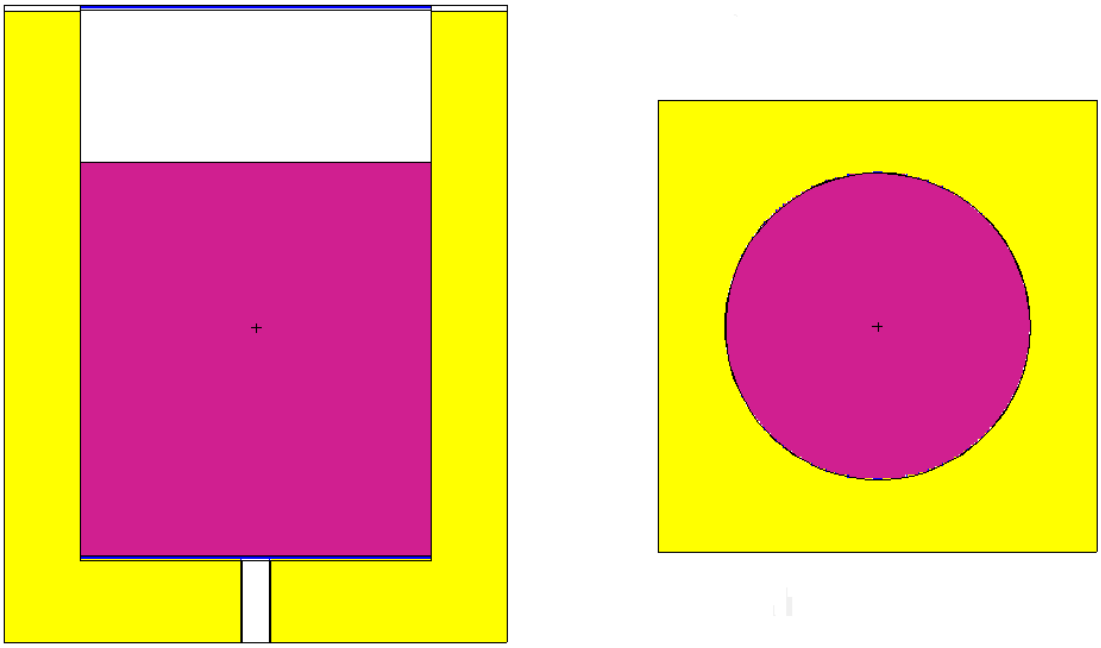

Figure 2. Criticality Benchmark MCNPX model

The next step was to consider the minor actinides, specifically the composition of minor actinides present in spent fuel which would then be reprocessed.

SPENT FUEL ACTINIDE MINIMUM CRITICAL MASS

Reprocessing streams typically contain mixtures of many different fissile isotopes, and the current UREX suite of reprocessing schemes requires the plutonium present in spent fuel to not be separated from the minor actinides for non-proliferation reasons. However, the specific break down of transuranic material in spent fuel depends on the fuel's life cycle and burn up.

A common descriptive tool is the plot of minimum critical mass vs. material concentration for a homogeneous mixture of fissile material and some moderator.

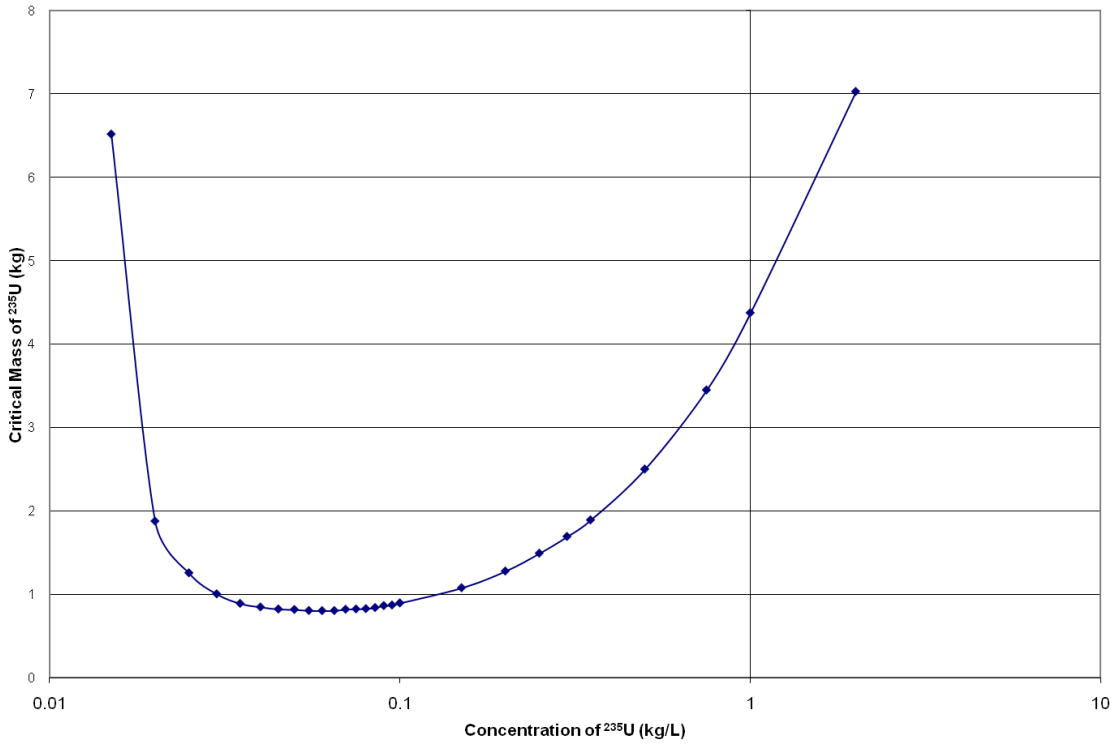

Figure 3. Minimum critical mass vs. concentration for a homogeneous mixture of ^{235}U and light water

For example, figure 3 is often seen in nuclear engineering textbooks and identifies the minimum critical mass for light water moderated ^{235}U at between 800-810 grams at a concentration of about 0.06 kg ^{235}U liter $^{-1}$ of solution. This plot was generated by simulating a bare sphere of the homogenous uranium/light water mixture. The critical

radius was found for a given concentration; just less than 11.6 cm for the lowest concentration, and the total mass of uranium in the system was calculated based on the concentration and the volume of the sphere. The process was then repeated for the next concentration.

A similar plot was generated for spent fuel of varying burn up. The minor actinide composition was generated using the IAEA Nuclear Fuel Cycle Simulation System, available at http://www-nfcis.iaea.org/NFCSS/NFCSSMain.asp, for a 1000 MWe PWR and 3.968% initially enriched fuel. Burnups of 25, 45, and 65 GWd tonne^{-1} were considered, as well as the composition of equilibrium cycle reprocessed fuel, as provided by Sandia National Laboratories researchers. The equilibrium composition represents the point in a closed fuel cycle at which point the isotopic make up of the reprocessed fuel ceases to change from cycle to cycle. The exact compositions used can be found in Appendix A.

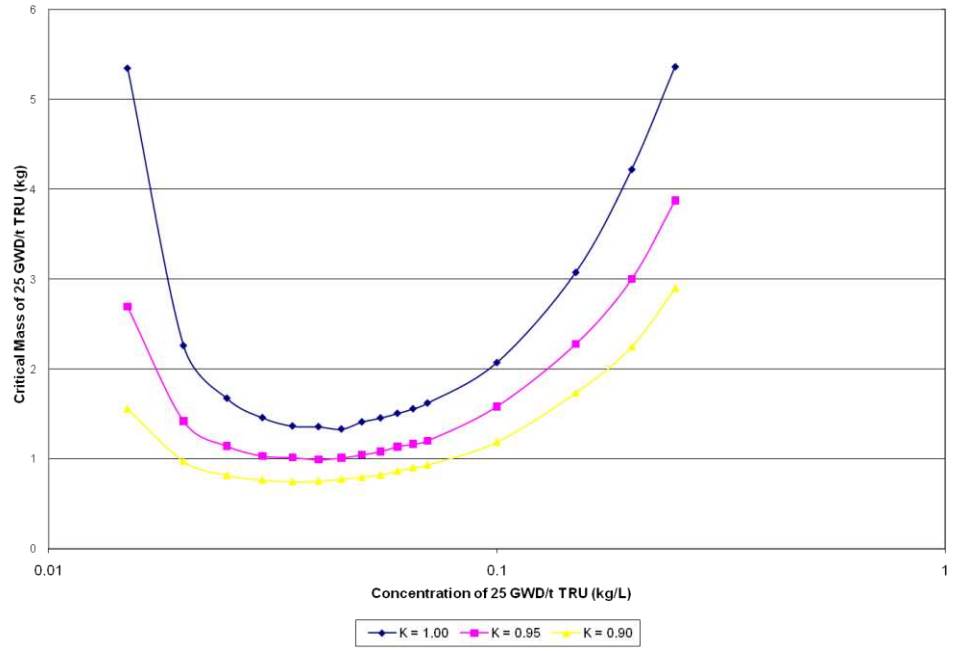

Figure 4. Minimum critical mass vs. concentration for a homogeneous mixture of 25 GWD t^{-1} TRU and light water

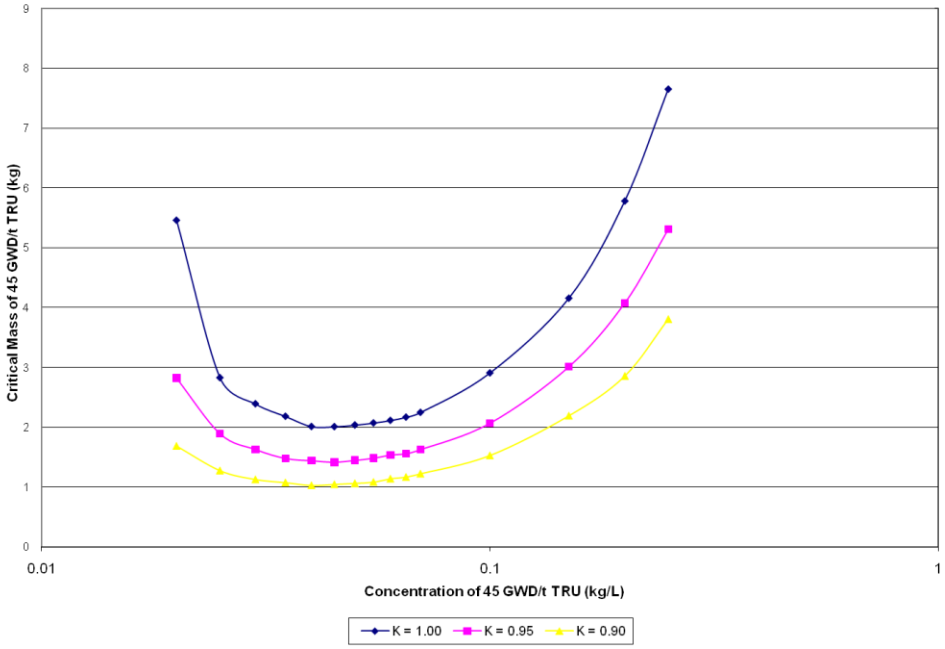

Figure 5. Minimum critical mass vs. concentration for a homogeneous mixture of 45 GWD t^{-1} TRU and light water

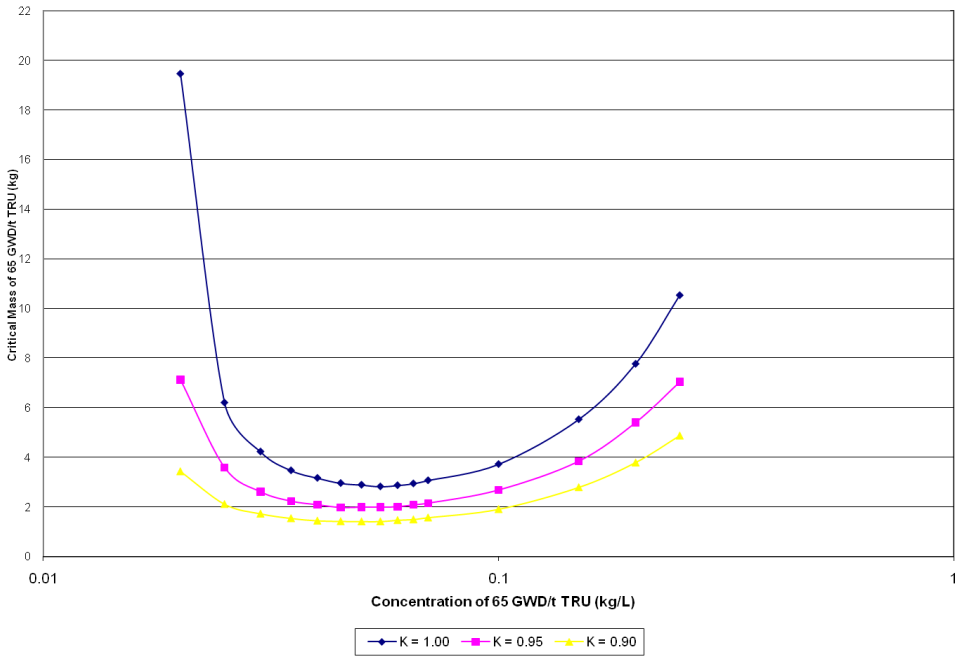

Figure 6. Minimum critical mass vs. concentration for a homogeneous mixture of 65 GWD t^{-1} TRU and light water

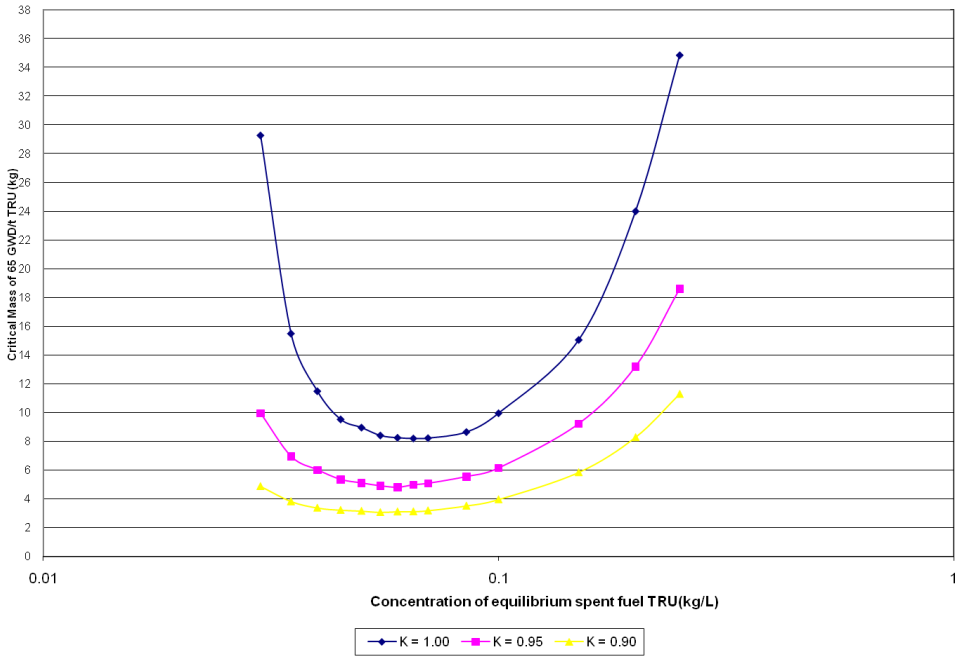

Figure 7. Minimum critical mass vs. concentration for a mixture of equilibrium cycle TRU and light water

As can be seen by the above plots, the critical mass for these mixtures of TRU isotopes was greater than for ^{235}U alone, though for the 25 GWD t^{-1} and 45 GWD t^{-1} spent fuel they occurred at a lower concentration of about 0.45 kg L^{-1}, while the 65 GWD t^{-1} and equilibrium cycle spent fuel's minimum critical mass occurred at about the same concentration as for pure ^{235}U. Experimental validation of these results could be achieved in a manner similar to the benchmark previously discussed. A closely measured volume of actual spent fuel minor actinides could be observed for criticality with a similar experimental set up. However, increased safety precautions would be required due to the dose concerns of handling the minor actinides.

Two points of interest arose from generating these plots. The first is the larger minimum critical mass of the equilibrium cycle fuel relative to the spent fuel. As seen in appendix A, the model for this fuel included more minor actinide isotopes than did the IAEA Nuclear Fuel Cycle Simulation System for the spent fuels. Additionally, this fuel contains less ^{239}Pu and ^{241}Pu than any of the spent fuels. While it is most likely the reduced amount of these fissile isotopes is primarily responsible for the increase in minimum critical mass, the inclusion of the other minor actinides might also have had an effect.

Secondly, when generating these plots the minimum critical radius decreased as the concentration of fissile materials increased, except for the last few data points. For example, for 65 GWd t^{-1} spent fuel the minimum critical radius at 0.2 kg L^{-1} concentration was 21.08 cm, while at 0.25 kg L^{-1} the minimum critical radius was 21.68 cm. This result seemed counter-intuitive and was more thoroughly investigated, however it held true in all of the mixed TRU cases. This would seem to indicate that at higher concentrations of fissile material neutron moderation is decreased to the point that more neutrons are absorbed while fast by the non- or less fissile transuranic elements present, as their absorption and fission cross-sections tend to be higher in the fast region. However, the upper concentrations modeled were far above those seen in actual reprocessing scenarios. Typical plutonium concentrations from dissolved LWR SNF are

on the order of 2 g L^{-1}, with minor actinide concentrations 30 times less than that of plutonium (Stanbro, 1997).

CONCLUSIONS

Based on the generated critical mass vs. concentration plots for the spent fuel minor actinides, current criticality safety controls for ^{235}U in solution should be sufficient for the considered mixes of minor actinides in solution, provided the controls are based on mass rather than concentration. These solutions of actinides would be present at the initial stages of reprocessing; more information would be needed about the particulars of a reprocessing scheme to address criticality safety issues further downstream when some isotopes may or may not be separated out.

Finally, it should be noted that as these results were obtained by MCNPX simulation, inaccuracies in the cross-section data used affect their accuracy. Improvements in interaction models or analysis of experimental data, particularly in the fission cross-section of these minor actinides should improve both the accuracy and usefulness of these results.

CHAPTER 3: MINOR ACTINIDE FISSION CROSS-SECTION CORRECTIONS

As the nuclear industry moves towards a closed fuel cycle increased attention has been paid to the accuracy of the current evaluated nuclear data for the minor actinides (Mengoni, *et al*, 2008). The purpose of this work was to create a simple method for identifying and predicting potential corrections to the high energy fission cross-sections of ^{237}Np, ^{238}Pu, ^{242}Pu, ^{241}Am, ^{243}Am, and ^{244}Cm. Corrections were obtained by regressing ENDF-derived spectrum-weighted multigroup cross sections onto the experimental results from central fission rate ratio experiments performed by the Japan Atomic Energy Agency (JAEA) in 8 test cores of varying spectral hardness (Okajima, *et al.*, 2008). The correction factors took the form of multiplicative constants applied to the multigroup cross sections. As the values of these constants was directly related to the energy group structure chosen, an iterative process was established where by many sets of constants were computed for different group structures. Using these overlapping group structures, the experimental energy range was characterized and a final correction function was estimated based on the behavior of the multiplicative constants.

JAPAN ATOMIC ENERGY AGENCY EXPERIMENTAL BASIS

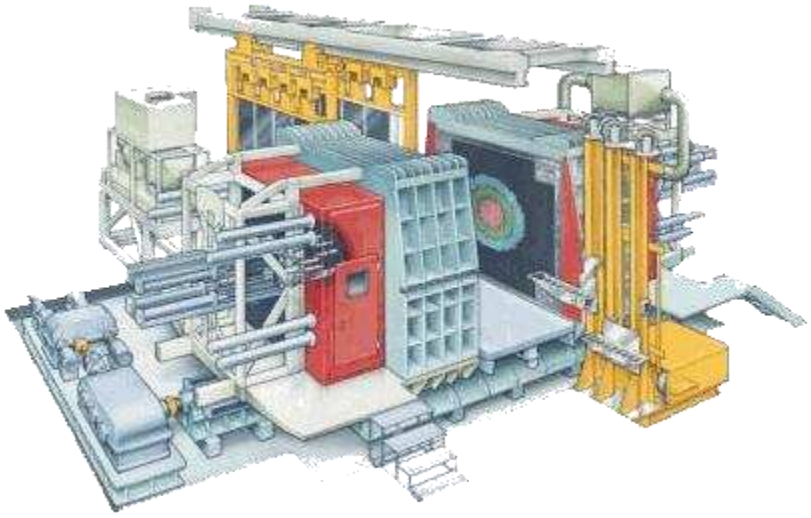

Figure 8. FCA facility whole view (JAEA Reactor Physics Group)

Between 1980 and 1982 the Japan Atomic Energy Agency (JAEA) completed a series of integral reaction rate ratio experiments at their Fast Critical Assembly (FCA) facility, seen above in figure 1. These experiments determined the ratio of the fission rate in several key minor actinides (^{241}Am, ^{243}Am, ^{244}Cm, ^{237}Np, ^{238}Pu, and ^{242}Pu) to the fission rate of ^{239}Pu in 8 test spectra of varying hardness.

The FCA facility is composed of two subcritical "half" assemblies, one fixed (seen below in figure 9) and the other mobile, each comprised of a grid of 51 x 51 "drawers" which can be hand loaded with reactor materials such as various actinide fuels, cladding material, and moderating material (Sasa, 2008). This design allows for great flexibility in core composition, geometry, and neutron spectrum. Once the desired geometry and material composition is completed the mobile half of the FCA is joined to the fixed face to achieve criticality.

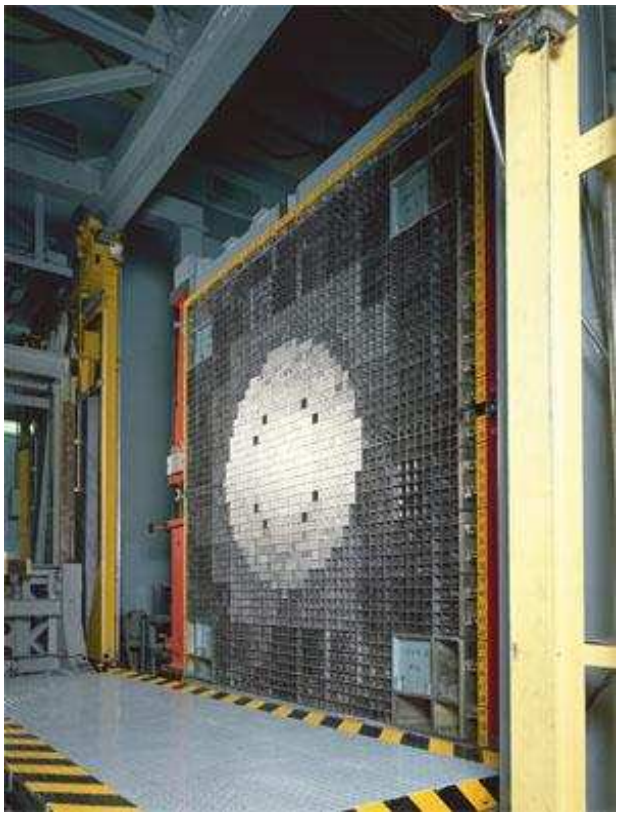

Figure 9. FCA fixed face (JAEA Reactor Physics Group)

The integral actinide fission ratio experiments were conducted by mounting a parallel plate type fission chamber in a cavity in the central fuel drawer, shown in figure 10. Foils coated with the actinides listed above were placed in the fission chambers, and their fission rate was measured while the assembly operated at a low critical power of 10-40 W, except in the case of the ^{244}Cm foil as the actinide's high rate of spontaneous fission required a power level of 200 W to reduce background. The fission rate of a ^{239}Pu coated foil was also measured. This process was repeated for each of 8 cores.

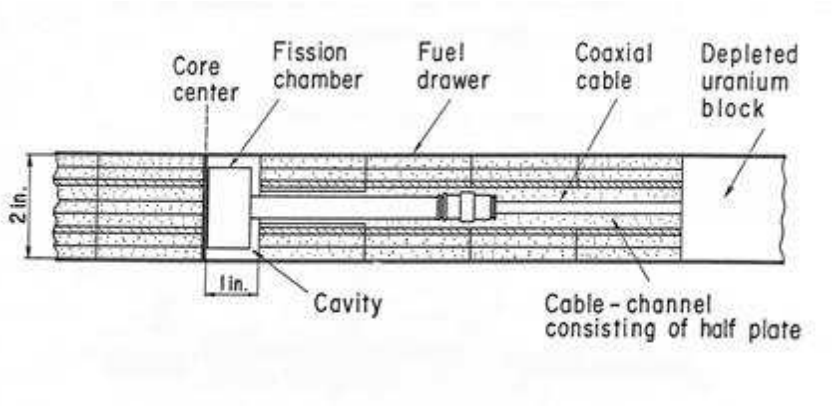

Figure 10. Fission chamber mounted in central fuel drawer (JAEA Reactor Physics Group)

These 8 cores were labeled as IX-1 through IX-7, and X1. The IX-1 through IX-6 cores were composed of high enriched uranium (93% enriched) with moderation provided by graphite in the IX-1 through IX-3 cores and stainless steel in the IX-4 through IX-6 cores. Spectrum hardness shifted from softer to harder in the order of the core number. The IX-7 core was composed of low enriched metal uranium only. The X-1 core was composed of high enriched uranium and plutonium with moderation provided by sodium. The IX-7 and X-1 core spectra were softer than the IX-6 but harder than the softest cores (Okajima *et al.,* 2008).

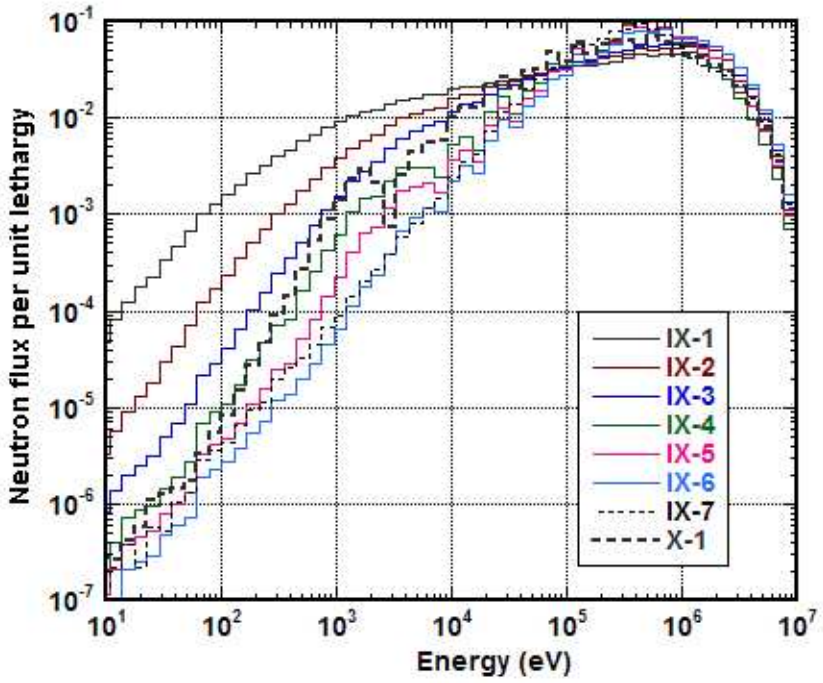

Figure 11. Calculated spectra at FCA core center

After correction for extrapolation-to-zero events and impurity fission events, the results of the central fission core reaction ratio were as tabulated below. It should be noted that the use of small actinide foils decoupled the neutron spectrum from uncertainty in the actinide fission cross section. The small sample size eliminated self-shielding within the actinide foil, and minimized the impact the fission of the sample itself had on the neutron spectrum.

Table 1. Measured results of central fission rate ratios in FCA cores

Core	^{237}Np / ^{239}Pu	^{238}Pu / ^{239}Pu
IX-1	0.2048 ±2.2%	0.5856 ±2.4%
IX-2	0.3145 ±2.6%	---/---
IX-3	0.3761 ±2.4%	0.8062 ±2.6%
IX-4	0.3438 ±2.4%	0.8128 ±2.6%
IX-5	0.3983 ±2.4%	0.8603 ±2.6%
IX-6	0.4579 ±1.9%	0.9114 ±2.6%
IX-7	0.3410 ±2.4%	0.8174 ±2.6%
X-1	0.3175 ±2.1%	0.7777 ±2.3%

Core	^{242}Pu / ^{239}Pu	^{241}Am / ^{239}Pu
IX-1	0.1584 ±2.2%	0.1961 ±2.2%
IX-2	0.2458 ±2.6%	0.3074 ±2.7%
IX-3	0.2901 ±2.4%	0.3604 ±2.4%
IX-4	0.2593 ±1.9%	0.2932 ±2.4%
IX-5	0.2994 ±1.9%	0.3502 ±2.4%
IX-6	0.3503 ±1.9%	0.4233 ±2.4%
IX-7	0.2528 ±2.4%	0.2903 ±2.4%
X-1	0.2389 ±2.4%	0.2870 ±2.5%

Core	^{243}Am / ^{239}Pu	^{244}Cm / ^{239}Pu
IX-1	0.1509 ±2.2%	0.2614 ±3.6%
IX-2	0.2346 ±2.6%	0.3778 ±3.8%
IX-3	0.2766 ±2.4%	0.4363 ±3.6%
IX-4	0.2207 ±2.4%	0.4024 ±3.6%
IX-5	0.2640 ±2.4%	0.4569 ±3.6%
IX-6	0.3236 ±2.4%	0.5155 ±3.8%
IX-7	0.2147 ±2.4%	0.3956 ±3.7%
X-1	0.2185 ±2.1%	0.3766 ±4.1%

The goal of this project was to compare the data in the above tables to the fission rates implied by the ENDF cross section data given the spectra shown in figure 11, and if disagreement was found to estimate both the magnitude and energy range of the necessary corrections to the ENDF data.

COMPUTATIONAL WORK

Using ENDF-B/VI.6 data, MCNPX was used to fold the spectra from each core with the fission cross section for each of the minor actinides, allowing for the calculation of fission rate ratios of the minor actinides to Pu-239 as predicted by the ENDF data. These simulated reaction rates differed from the experimental reaction rates by up to 9.3%.

Table 2. MCNPX simulated reaction rates ratios and difference from experimental values.

Core	^{237}Np / ^{239}Pu	^{238}Pu / ^{239}Pu
IX-1	0.2029 -0.90%	0.5818 -0.65%
IX-2	0.3185 +1.26%	0.7384 / NA
IX-3	0.3617 -3.82%	0.7920 -1.76%
IX-4	0.3330 -3.16%	0.7893 -2.89%
IX-5	0.3836 -3.70%	0.8334 -3.12%
IX-6	0.4540 -0.85%	0.8895 -2.40%
IX-7	0.3365 -1.32%	0.7973 -2.46%
X-1	0.3081 -2.97%	0.7505 -3.49%

Core	^{242}Pu / ^{239}Pu	^{241}Am / ^{239}Pu
IX-1	0.1715 +8.26%	0.1928 -1.70%
IX-2	0.2687 +9.31%	0.3021 -1.72%
IX-3	0.3043 +4.91%	0.3380 -6.22%
IX-4	0.2749 +6.03%	0.2842 -3.08%
IX-5	0.3164 +5.69%	0.3318 -5.25%
IX-6	0.3770 +7.63%	0.4125 -2.55%
IX-7	0.2728 +7.91%	0.2822 -2.78%
X-1	0.2539 +6.28%	0.2740 -4.52%

Core	^{243}Am / ^{239}Pu	^{244}Cm / ^{239}Pu
IX-1	0.1463 -3.05%	0.2646 +1.24%
IX-2	0.2303 -1.85%	0.4011 +6.16%
IX-3	0.2568 -7.15%	0.4538 +4.01%
IX-4	0.2107 -4.52%	0.4181 +3.91%
IX-5	0.2466 -6.61%	0.4787 +4.78%
IX-6	0.3117 -3.69%	0.5616 +8.94%
IX-7	0.2090 -2.64%	0.4212 +6.48%
X-1	0.2056 -5.91%	0.3873 +2.83%

As can be seen in table 2, the ENDF data for ^{237}Np and ^{238}Pu seem to be reasonably accurate, while the data for the remaining four minor actinides appears to be in greater disagreement with the measurements. It was desirable to identify the energy groups where erroneous nuclear data was inducing the discrepancy and to estimate the magnitude of the error. It should be noted that uncertainties in the calculation of the eight experimental spectra may exist, however these are unknown at this time and the following analysis makes the assumption that the spectral uncertainty is low enough to be negligible. If possible, it would be ideal to include and propagate this source of uncertainty.

Given that there were only eight data points for each actinide except for ^{238}Pu which had 7 data points, it was necessary to use a very coarse group structure to ensure the resulting system of equations was sufficiently over determined, therefore it was decided to break up the energy range of the experimental data into four groups. MCNPX was then used to tally the fission rate in each of those groups for each actinide in each spectrum. The fission rate of ^{239}Pu was also tallied for each spectrum, as the experimental results are reported as the fission ratio of the actinide to ^{239}Pu. For the purpose of this analysis it was necessary to assume that any error in the ^{239}Pu cross-section was negligible compared to error in the actinide cross-section. Each group cross-section was then multiplied by a constant to be determined, referred to as λ_4 through λ_1. Therefore for each actinide each group cross-section was constrained to be incorrect by the same factor in each of the 8 cases, as shown in equation 1. In this equation $\phi_{i,j}$ [n/cm^2/s] is the ith group flux for the jth experimental trial, $\hat{\sigma}_{i,j}$ is the spectrum-weighted cross section obtained via an MCNPX-assisted group collapse of the ENDF data and RR_j is the measured reaction rate reported in Okajima, *et al.*

$$\min \sum_{j=1}^{8} \left(\left[\sum_{i=1}^{4} \lambda_i \hat{\sigma}_{i,j} \phi_{i,j} \right] - \left[RR_j \right] \right)^2 \qquad (1)$$

Regressions were carried out on the over determined system of equations given above to obtain the λ that led to the best fit of the modified minor actinide group cross-sections to the experimental values inferred from the reaction rates. This process was repeated for ^{237}Np, ^{241}Am, and ^{243}Am using ENDF/B-V data to verify that nuclear data has progressed in the direction of greater accuracy.

Initially the group structure of 10 ev – 1 keV, 1 keV – 100 keV, 100 keV – 1 MeV, 1 MeV – 10 MeV was selected. To demonstrate, the λ values resulting from this group structure and the effect of those constants when applied to the simulated fission reaction rate ratios for ^{237}Np and ^{243}Am are shown in tables 3 and 4 and figures 5 and 6 respectively.

Table 3. ^{237}Np lambda values for ENDF-B/VI.6

λ_4	1.0000
λ_3	1.0001
λ_2	1.0151
λ_1	1.0241

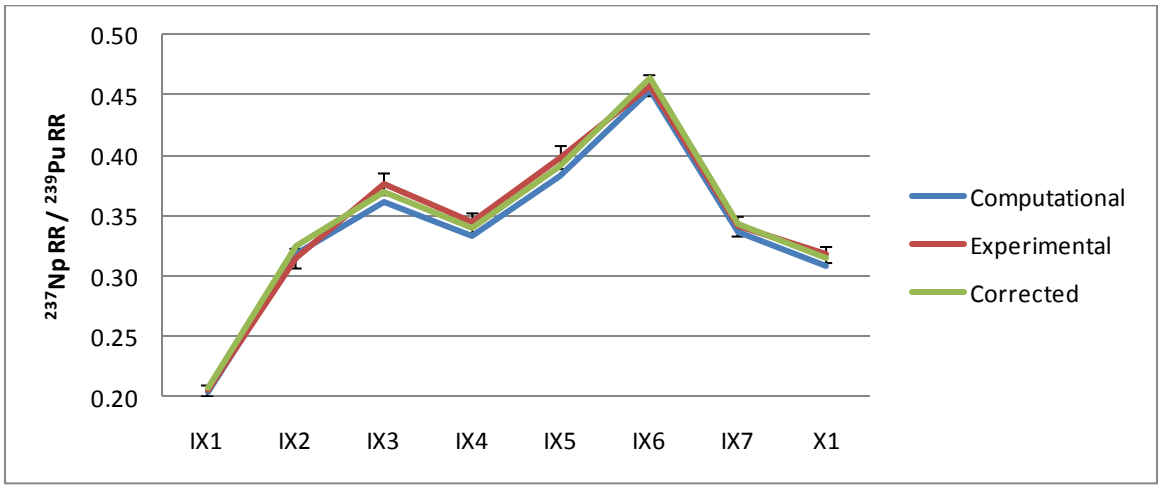

Figure 12. Experimental and λ-corrected CFRR for ^{237}Np, ENDF-B/VI.6

Table 4. ^{243}Am lambda values for ENDF-B/VI.6

λ_4	1.0000
λ_3	1.0004
λ_2	1.009
λ_1	1.0551

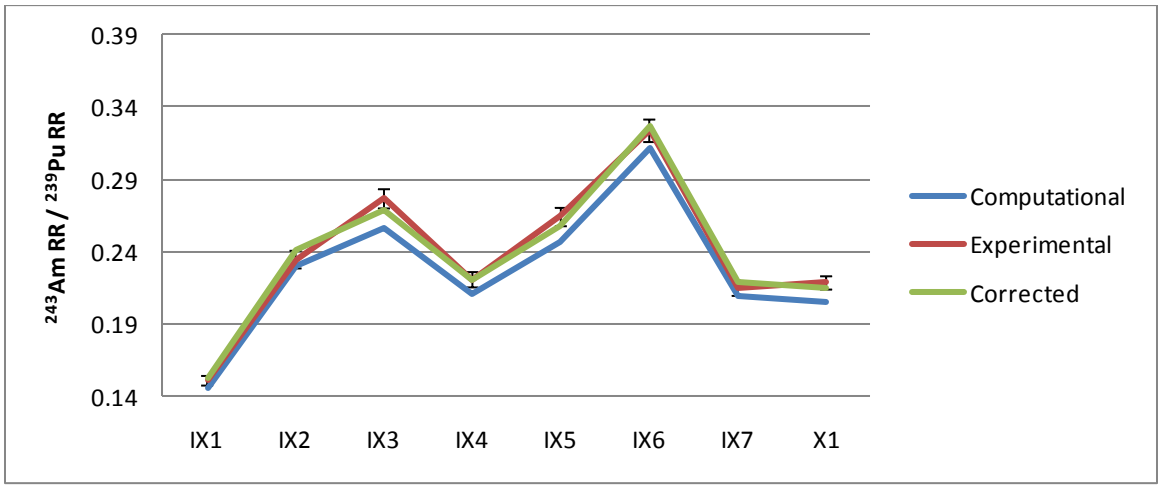

Figure 13. Experimental and λ-corrected CFRR for ^{243}Am, ENDF-B/VI.6

The λ values for the same group structure were also calculated using ENDF-B/V data to investigate the relative fidelity of the evaluations. These are shown in tables 5 and 6 and figures 7 and 8. The results for ^{237}Np appear to be within the margin of error for the experimental data, just under 2.5% for ENDF-B/VI.6 data in the highest energy group and around 1.5% in the same energy group for ENDF-B/V data. However, for Am-243 the suggested correction is greater than the margin of experimental error. For the same group structure for ^{243}Am, the ENDF-B/VI.6 data appears to undershoot the actual fission cross-section by 5 percent in the highest energy region, while the ENDF-B/V data appears to overshoot in the same region by nearly 9 percent.

Table 5. ^{237}Np lambda values for ENDF-B/V

λ_4	1.0000
λ_3	0.9999
λ_2	0.9938
λ_1	0.9873

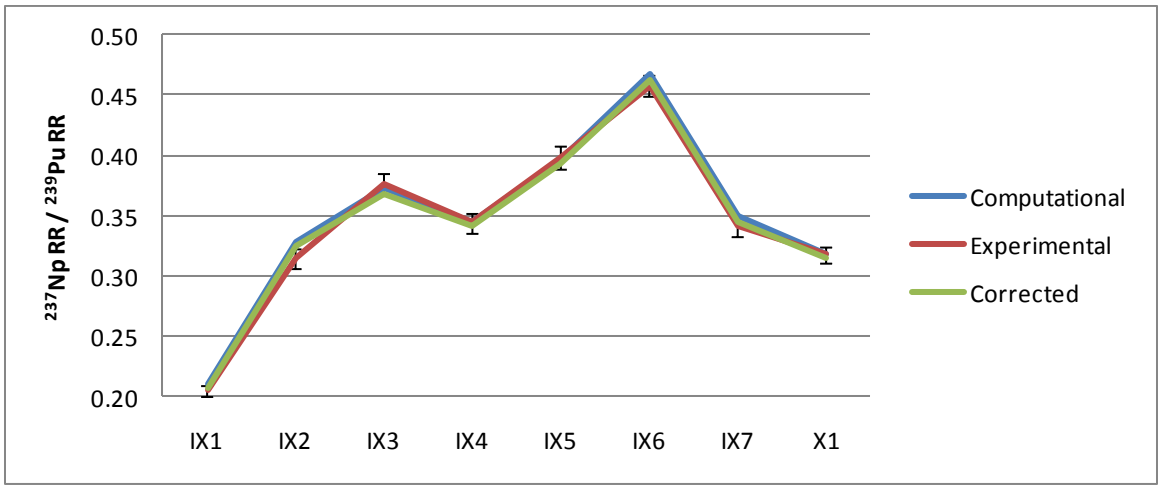

Figure 14. Experimental and λ-corrected CFRR for ^{237}Np, ENDF-B/V

Table 6. ^{243}Am lambda values for ENDF-B/V

λ_4	1.0000
λ_3	0.9993
λ_2	0.9812
λ_1	0.9110

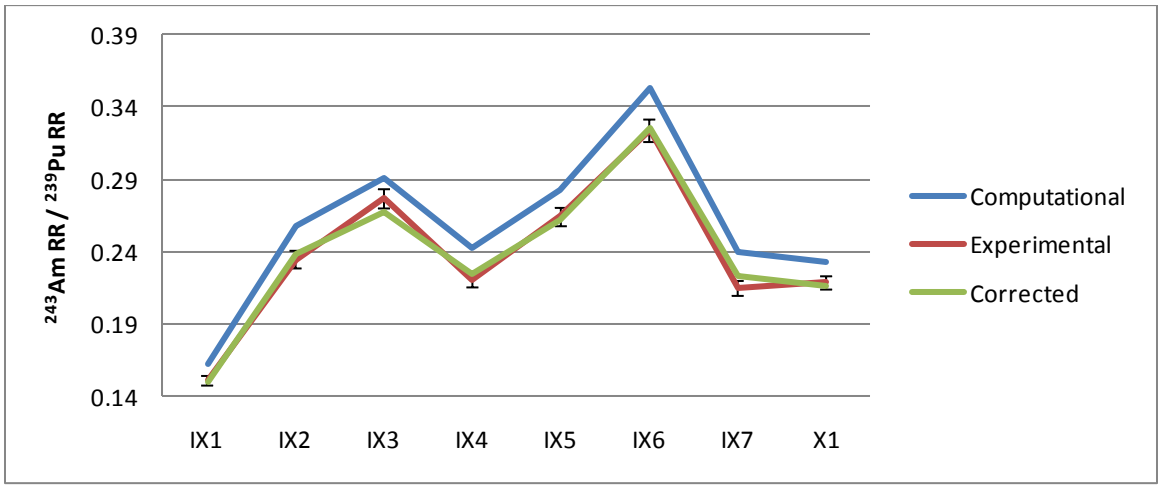

Figure 15. Experimental and λ-corrected CFRR for ^{243}Am, ENDF-B/V

For the sake of further clarity, figures 16 and 17 illustrates the MCNPX spectrum weighted group collapse of the ENDF-B/VI.6 data when using this group structure, as well as the correction obtained when the λ values are applied to the group cross-sections, though on a logarithmic axis this is difficult to see clearly.

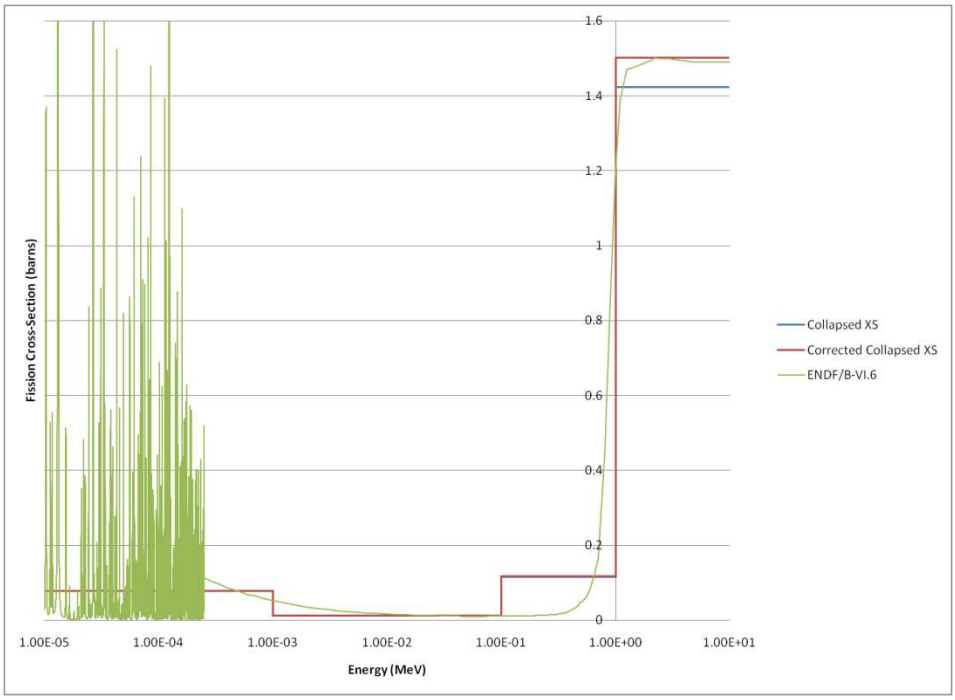

Figure 16. ENDF-B/VI.6 group collapse for ^{243}Am, linear vertical axis

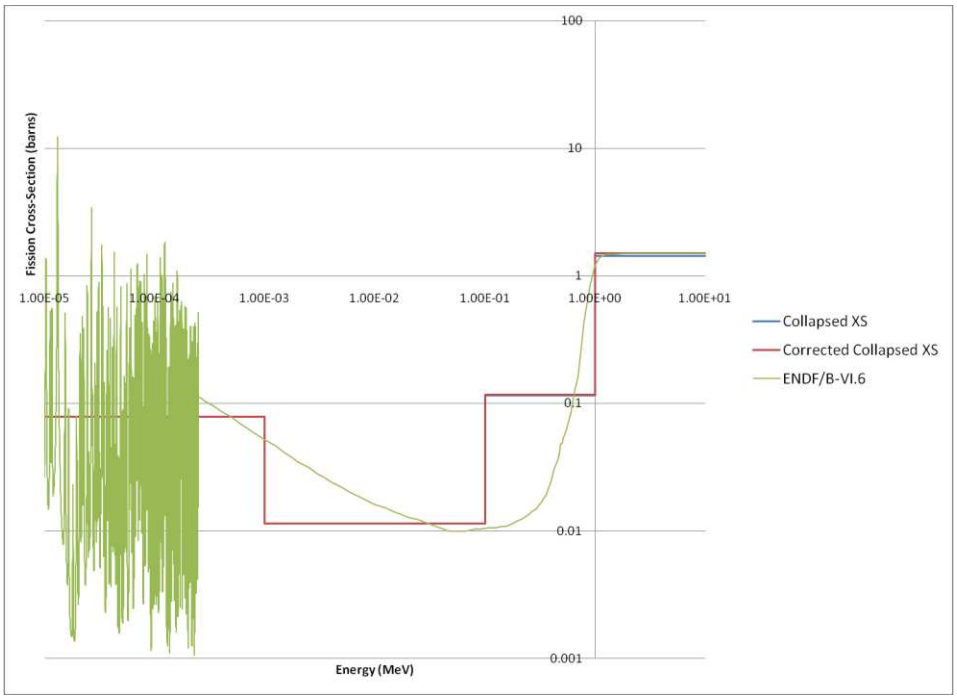

Figure 17. ENDF-B/VI.6 group collapse for ^{243}Am, logarithmic vertical axis

However, there is no way of knowing that these cross-section corrections are correct, as the group structure is necessarily coarse given the small set of data points. The λ values calculated are directly tied to the group structure chosen, so varying the group structure will result in different values for the four λs. By iterating on the above process, and calculating many sets of λ values for different group structures spanning the energy range of interest, it should be possible to generate a final correction function by fitting a curve to the calculated multiplicative constants.

The resulting λ values for 10 group structures for ^{237}Np and ^{243}Am are plotted in figures 18 and 19. Many appear to follow a pattern, indicating certain energy ranges where current evaluated nuclear data may be incorrect. Indeed, many of the actinide cross-sections seem to be in error in the region of the fission threshold.

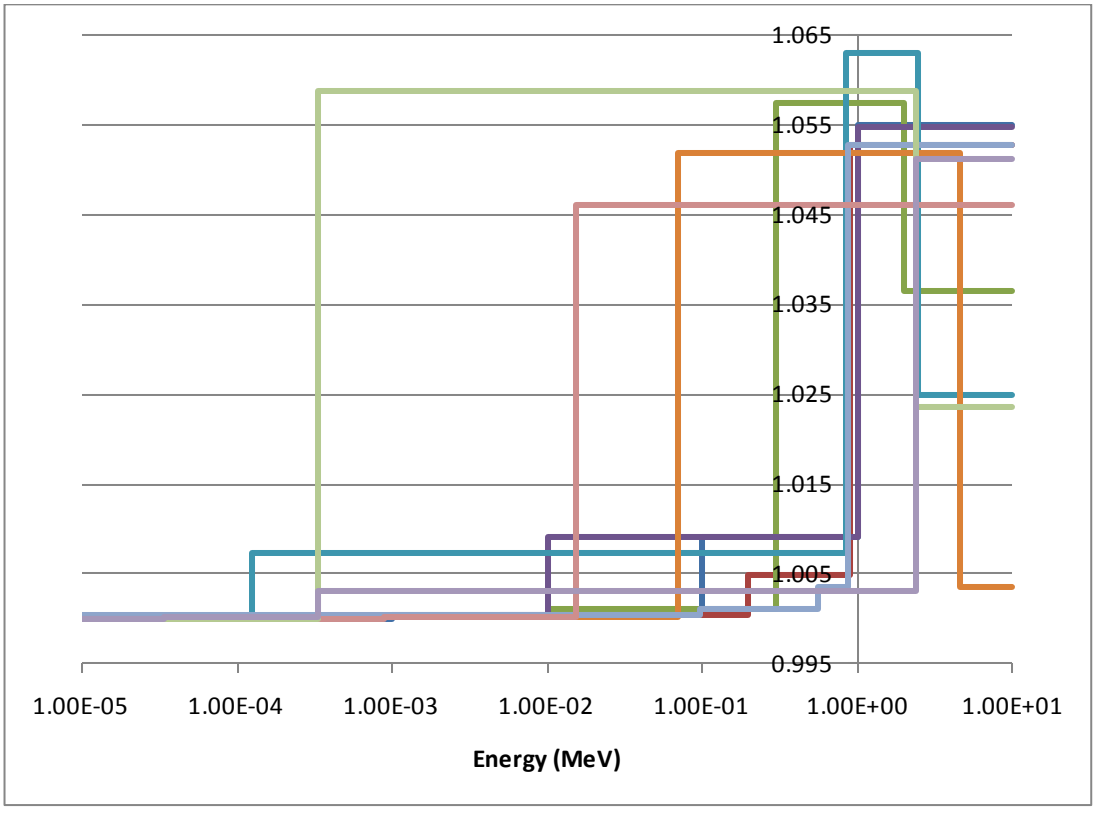

Figure 18. λ values for 10 different group structures for ^{243}Am

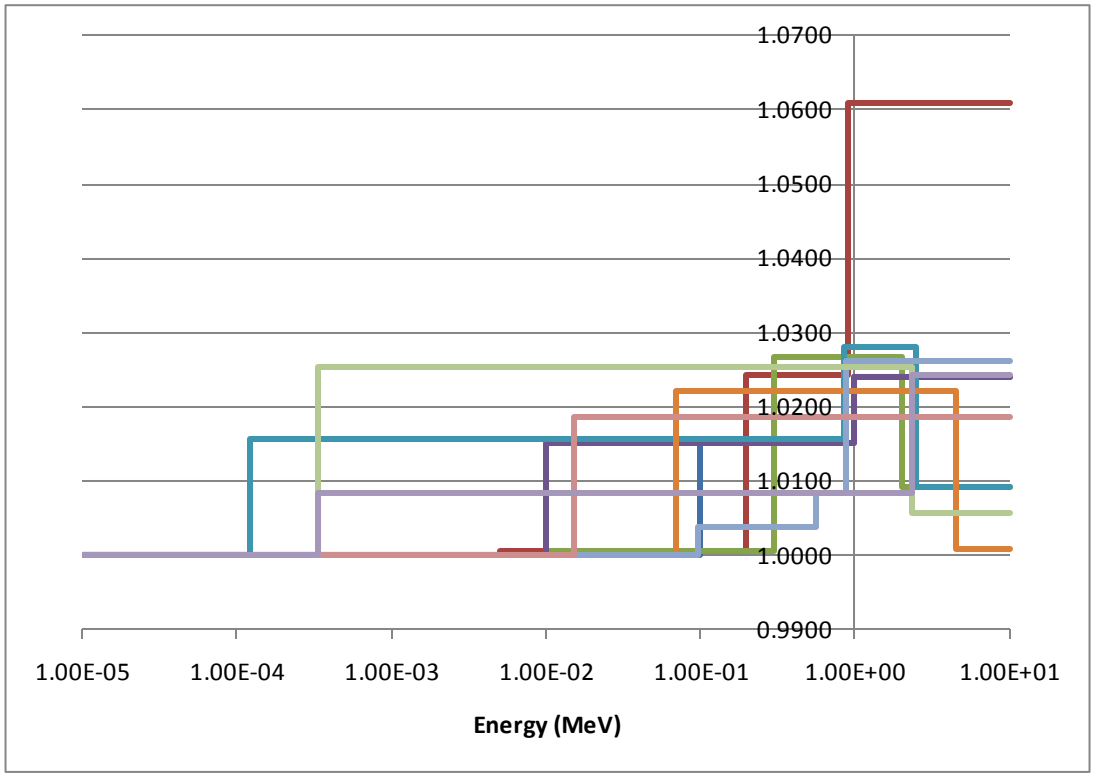

Figure 19. λ values for 10 different group structures for ^{237}Np

While many of the lambda value sets for the actinides appear to follow a general pattern, there is also a good deal of "noise" in the resulting plots. To this point there has not been a discussion of the goodness of fit of the particular lambda values to the experimental data. This has been primarily due to the fact that the length of time needed to generate one set of lambda values was prohibitive to compiling enough sets to discriminate between them. However, this problem was surmountable.

As can be seen in figure 11, the experimental spectra were reported themselves as a somewhat coarse group structure, consisting of 56 logarithmically spaced groups. The next step in this analysis was to use MCNPX to calculate a reaction rate for each of those 56 groups for each experimental spectrum for each actinide. Using this data, the time needed to generate lambda correction sets was vastly reduced as the coarser 4-group boundaries could be easily varied.

The 56 relative reaction rate data could be collapsed into a 4 group structure by specifying three of the groups within the 56 group structure and summing the reaction rates of all the groups between these chosen "end-points." Once this collapsed 4 group structure was obtained, the corrective lambda values could be calculated as before. By randomly varying this group collapse using MATLAB, 100 sets of lambda values could be generated in under a minute, as compared to 2 hours of MCNPX run time for each of the 8 spectra for a single set of lambda values previously.

Additionally, with this larger sample size available, the lambda sets could be ranked based on their R-square goodness of fit values. Taking the top 10 best fit lambda value sets for each actinide from 100 randomly generated group structures results in the following plots. Also included are plots of the relative actinide reaction rates as compared to Pu-239 throughout the energy range.

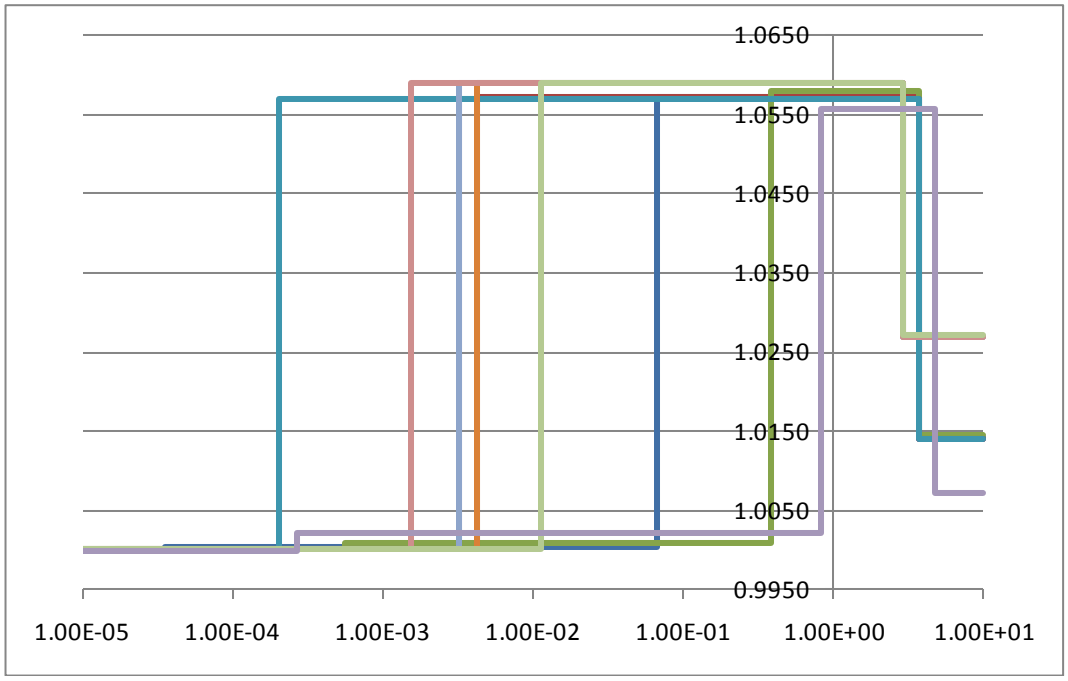

Figure 20. ^{243}Am Top 10 best fit lambda sets

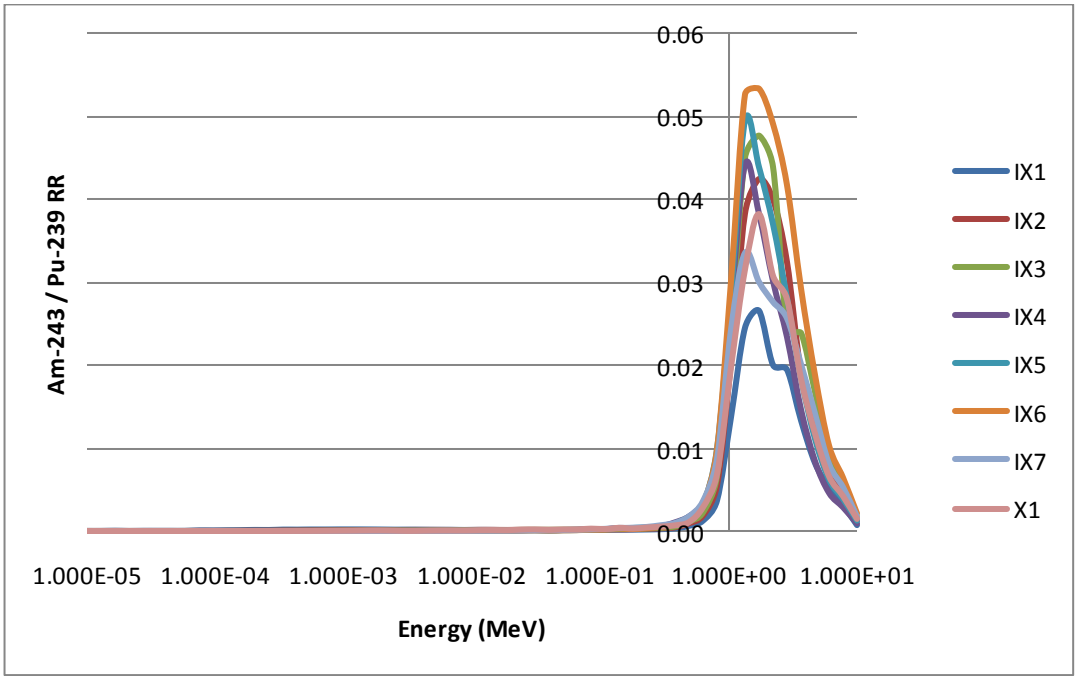

Figure 21. ^{243}Am / ^{239}Pu relative reaction rate over the experimental energy range

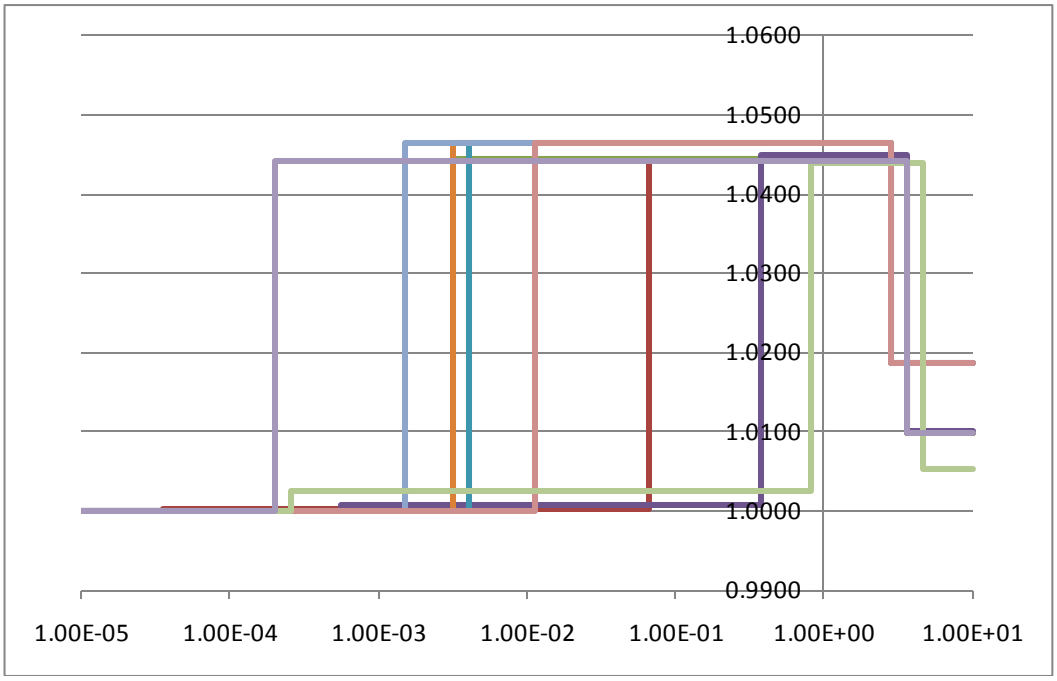

Figure 22. ^{241}Am Top 10 best fit lambda sets

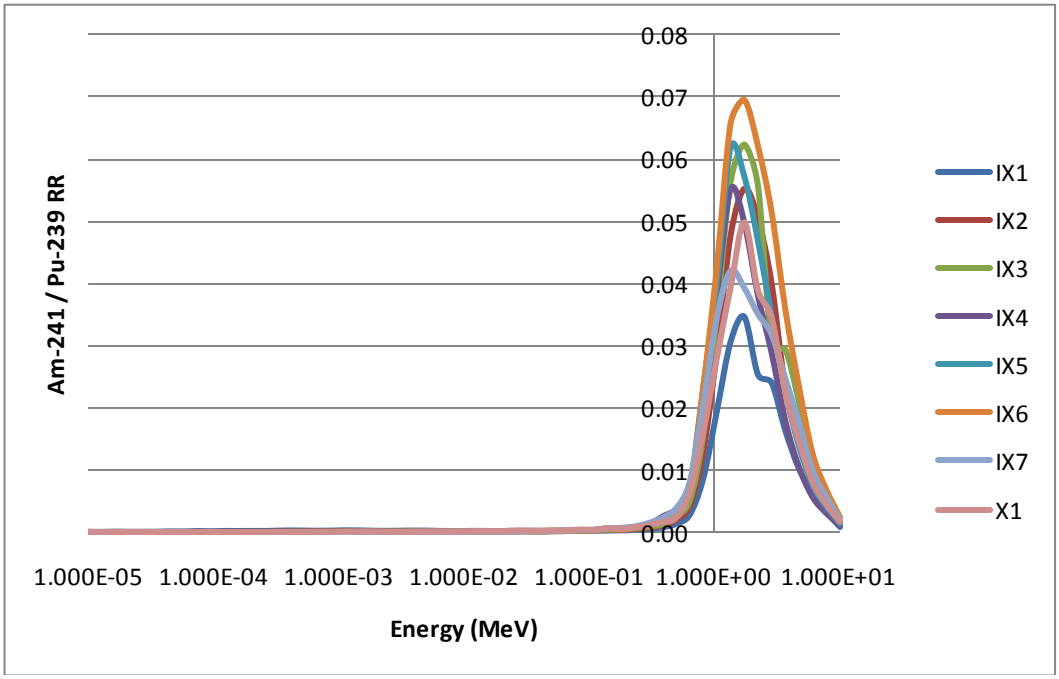

Figure 23. ^{241}Am / ^{239}Pu relative reaction rate over the experimental energy range

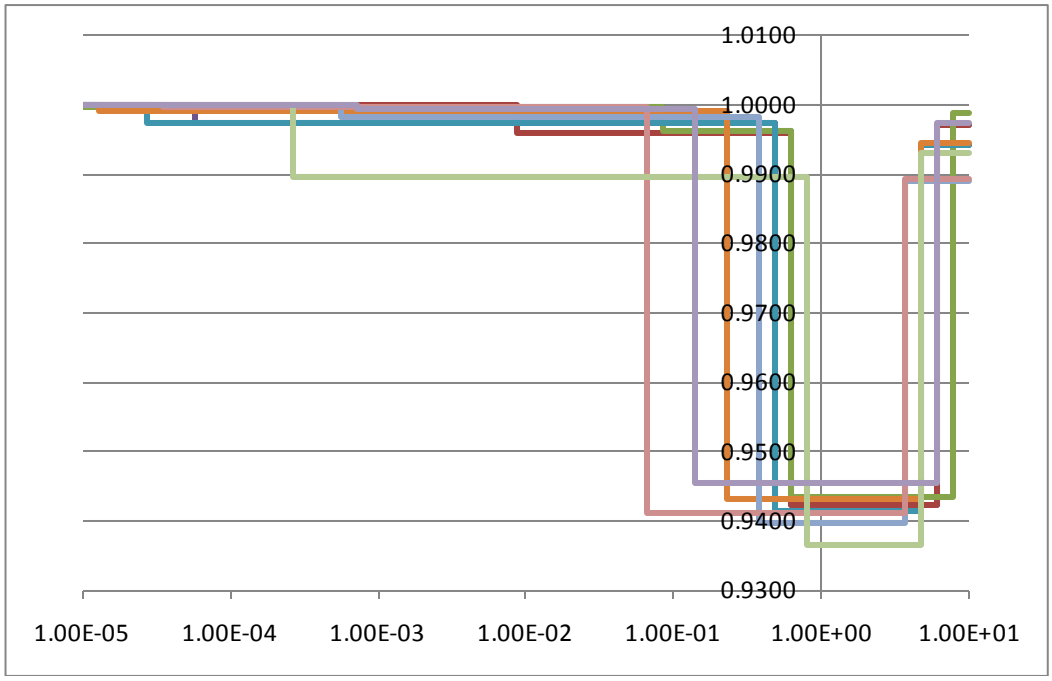

Figure 24. ^{244}Cm Top 10 best fit lambda sets

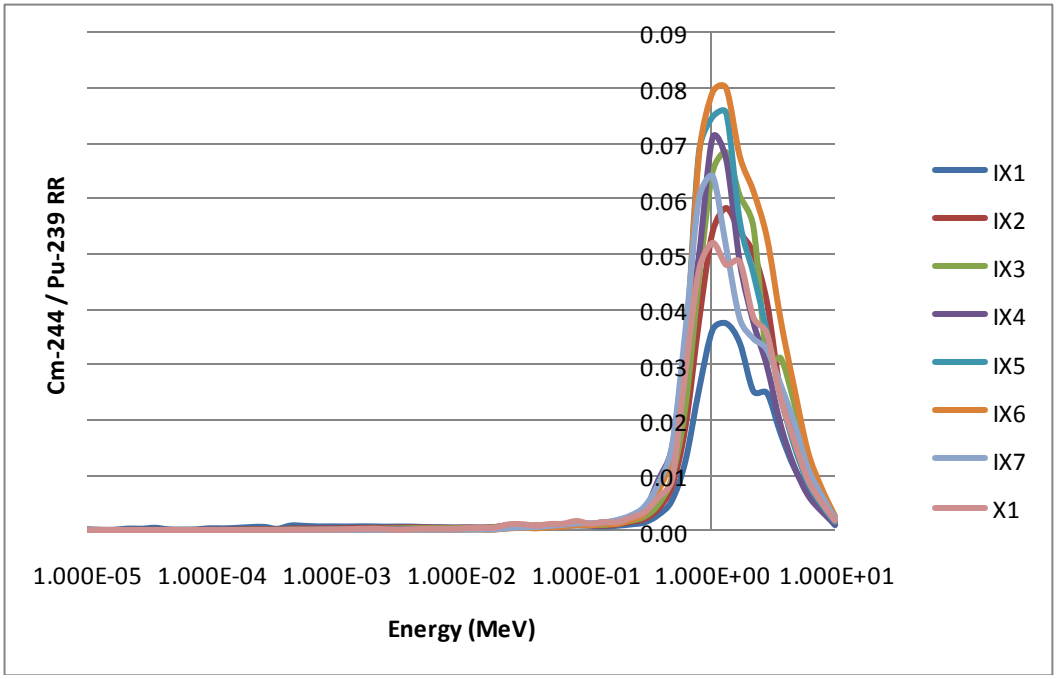

Figure 25. ^{244}Cm / ^{239}Pu relative reaction rate over the experimental energy range

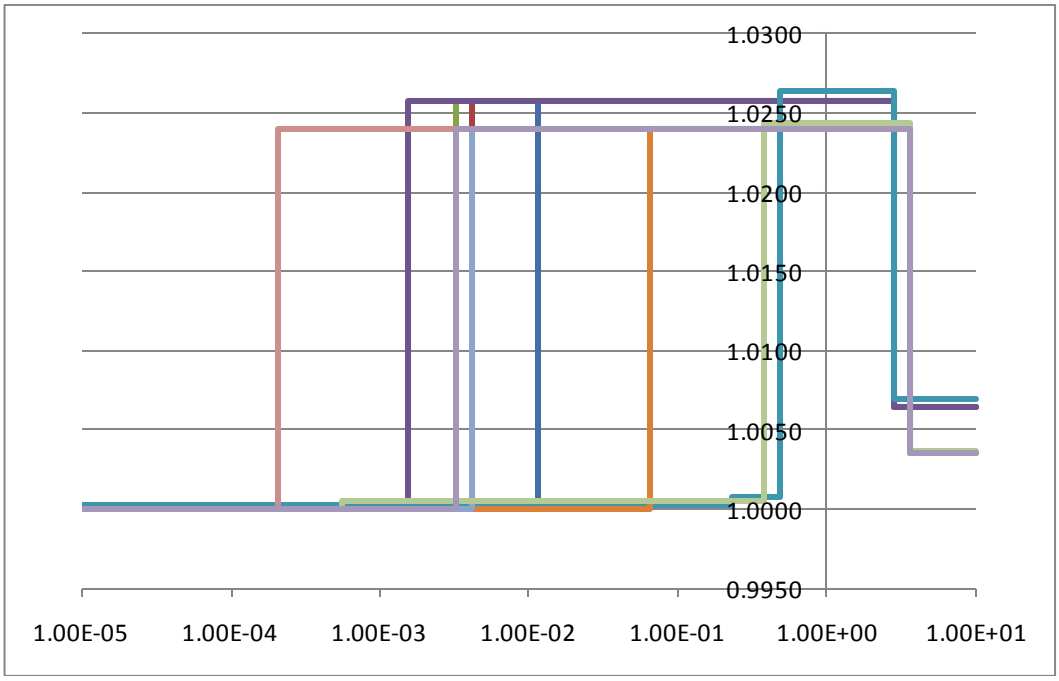

Figure 26. ^{237}Np Top 10 best fit lambda sets

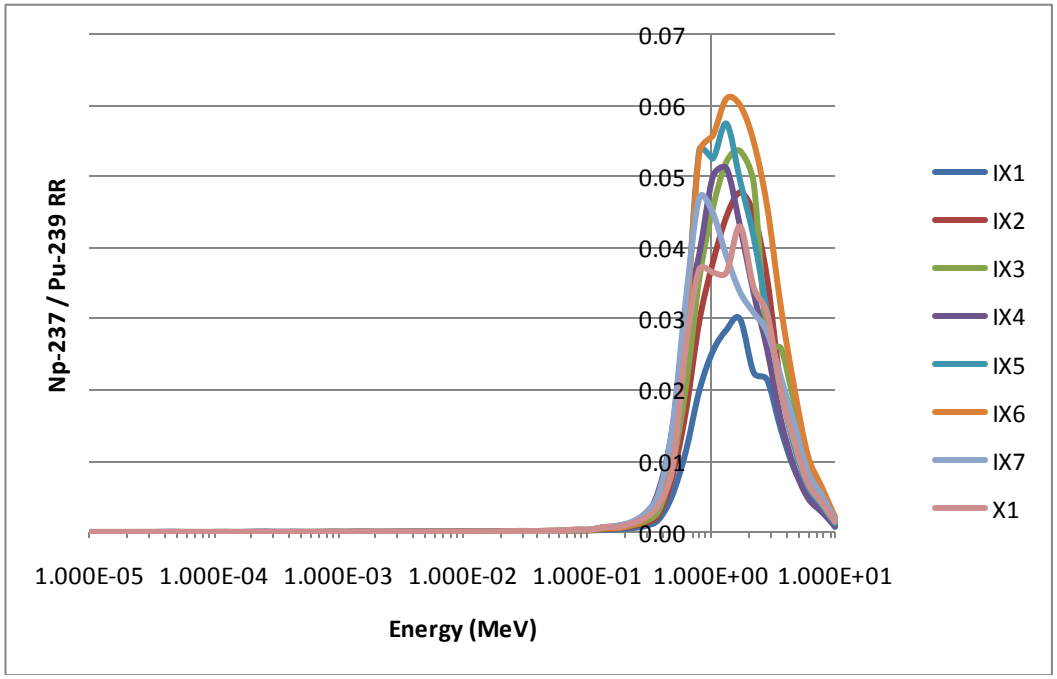

Figure 27. ^{237}Np / ^{239}Pu relative reaction rate over the experimental energy range

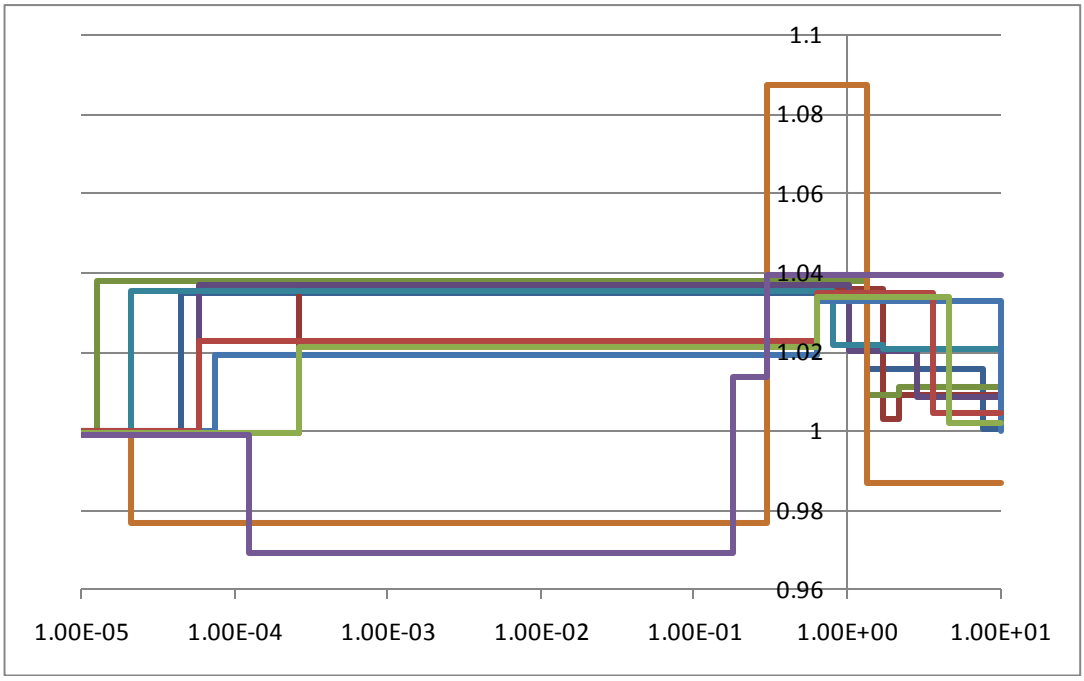

Figure 28. ^{238}Pu Top 10 best fit lambda sets

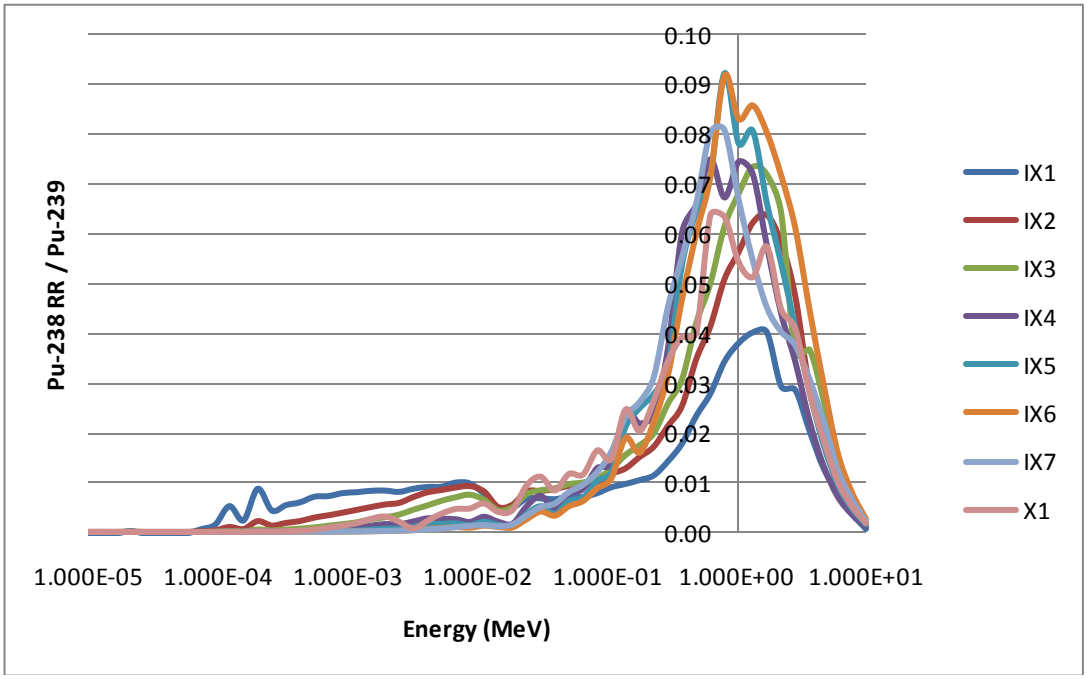

Figure 29. ^{238}Pu / ^{239}Pu relative reaction rate over the experimental energy range

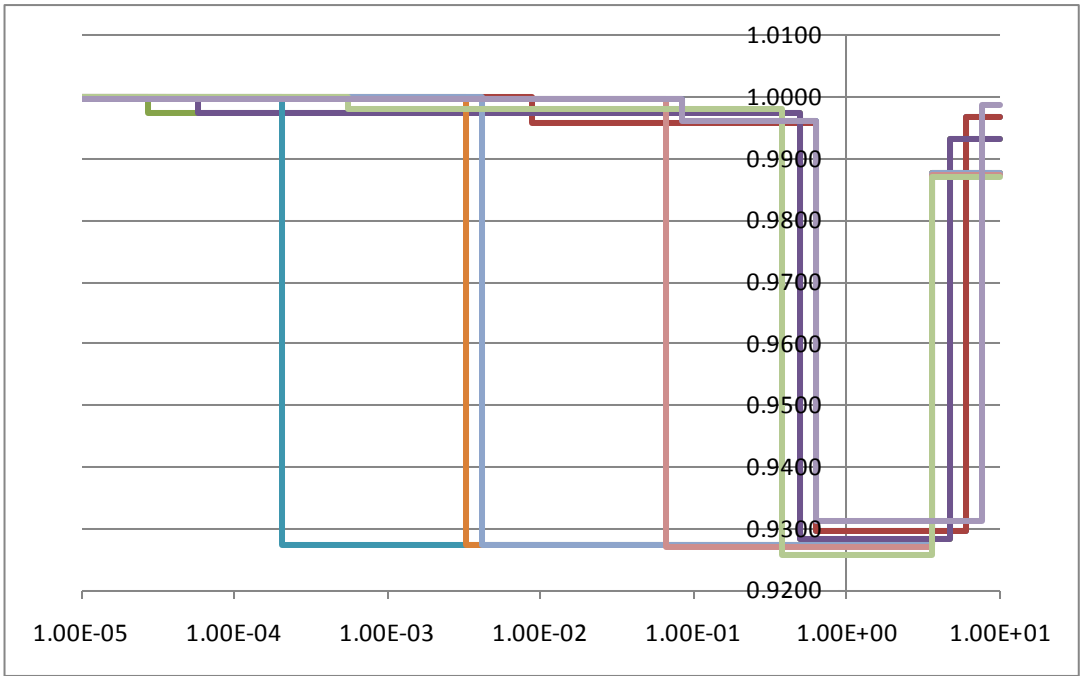

Figure 30. ^{242}Pu Top 10 best fit lambda sets

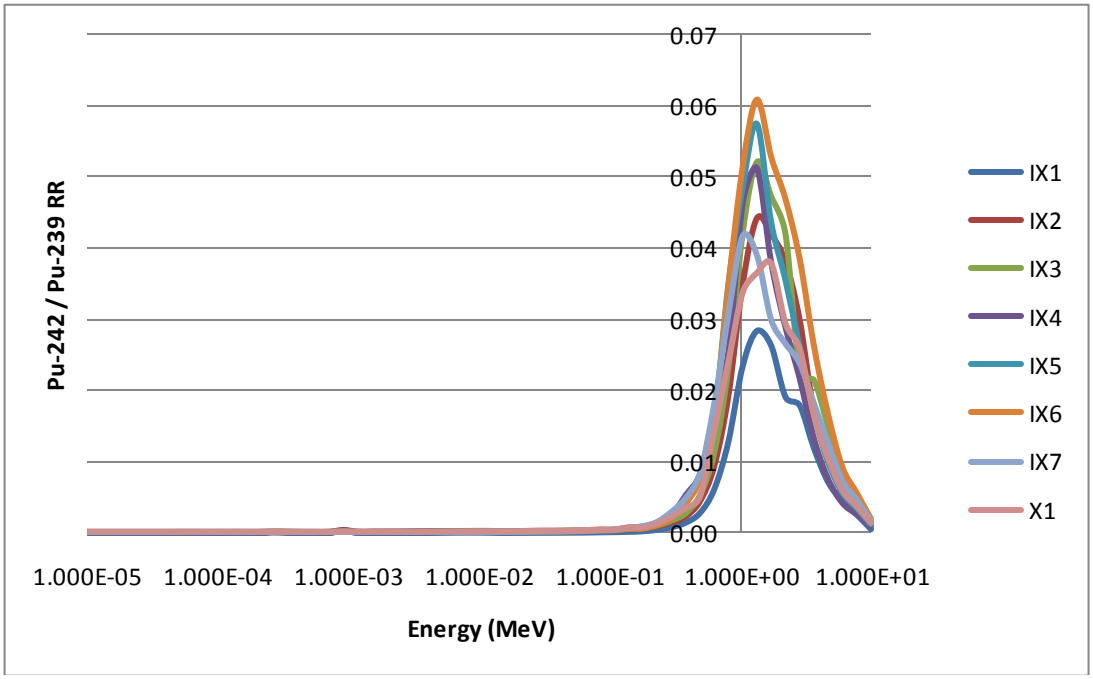

Figure 31. ^{242}Pu / ^{239}Pu relative reaction rate over the experimental energy range

ANALYSIS OF RESULTS

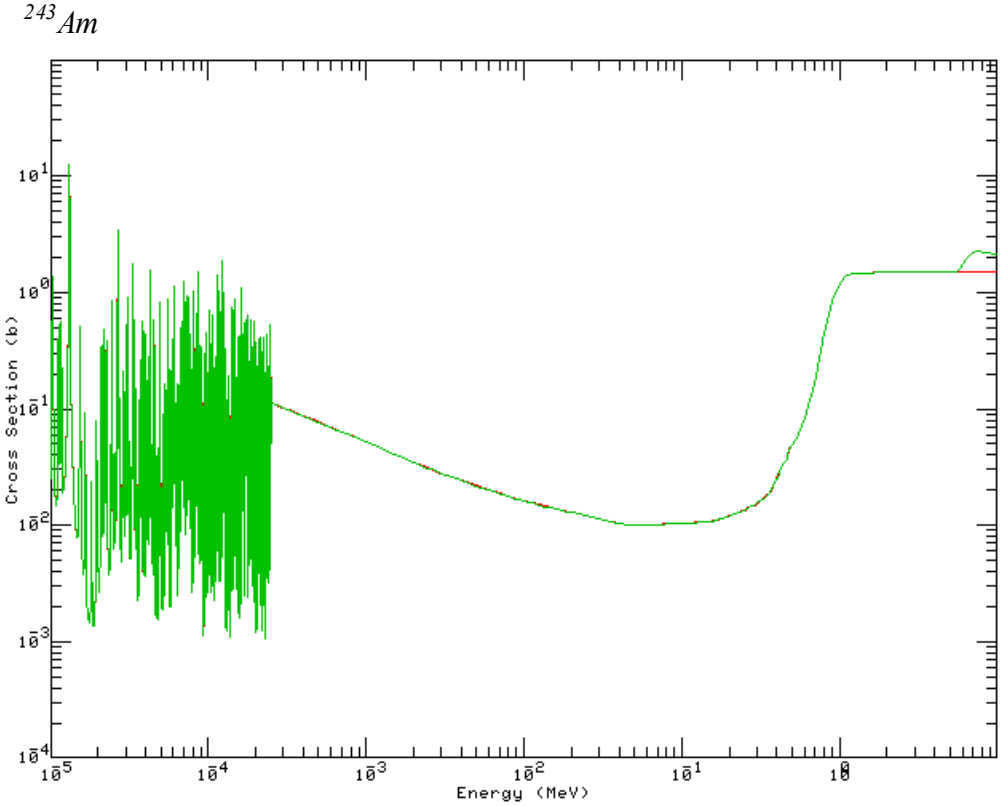

Figure 32. ^{243}Am ENDF-VI.6 first chance fission cross section (red) and UKAEA EVAL_JUL-03 total fission (green)

As can be seen in figure 21, there is practically no ^{243}Am fission relative to ^{239}Pu fission below about 1 MeV, roughly corresponding to the fast fission threshold (fig.24). Therefore lambda values below this energy can be neglected, as they do not influence the overall fit of the computational results to the experimental data. Considering this, figure 12 seems to suggest that while the fast fission threshold is placed correctly in the energy domain, the plateau cross-section value above the threshold is low by between 5.5% and 6%.

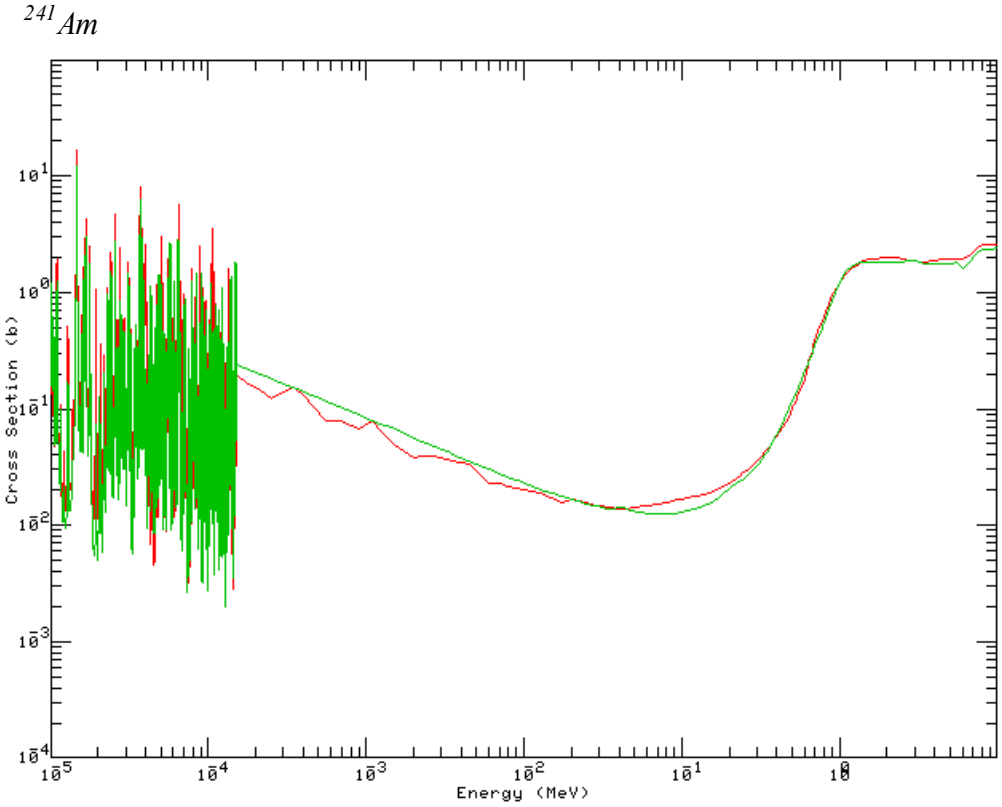

Figure 33. ^{241}Am ENDF-VI.6 fission cross section (red) and UKAEA EVAL JUL-03 (green)

The results for ^{241}Am are very similar to those seen for ^{243}Am: minimal relative fission activity below the threshold as seen in figure 23, and a suggested correction to the plateau cross-section value just above the fast fission threshold of 4.5%.

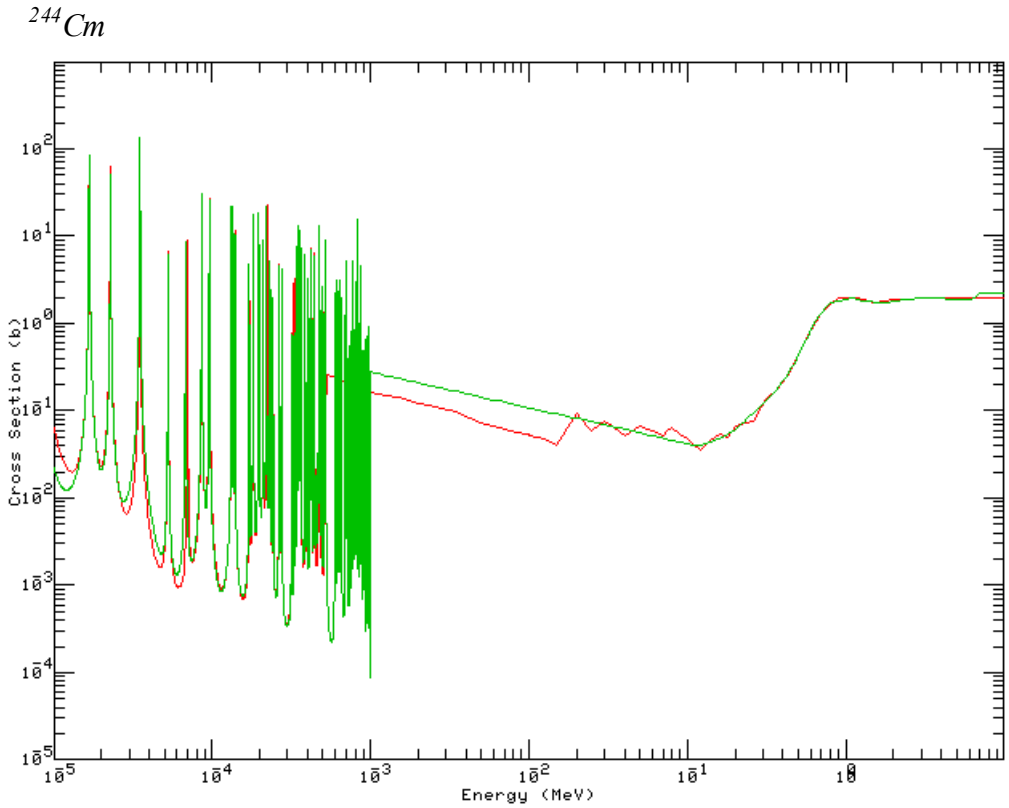

Figure 34. ^{244}Cm ENDF-VI.6 first chance fission cross section (red) and UKAEA EVAL_JUL-03 total fission (green)

Again, as seen in figure 17, ^{244}Cm has practically no relative fission activity below the fast fission threshold value of about 500 keV (fig. 34). However, unlike the americiums, the suggested correction to the ^{244}Cm fast fission plateau is a decrease of between 5.5% and 6.5%.

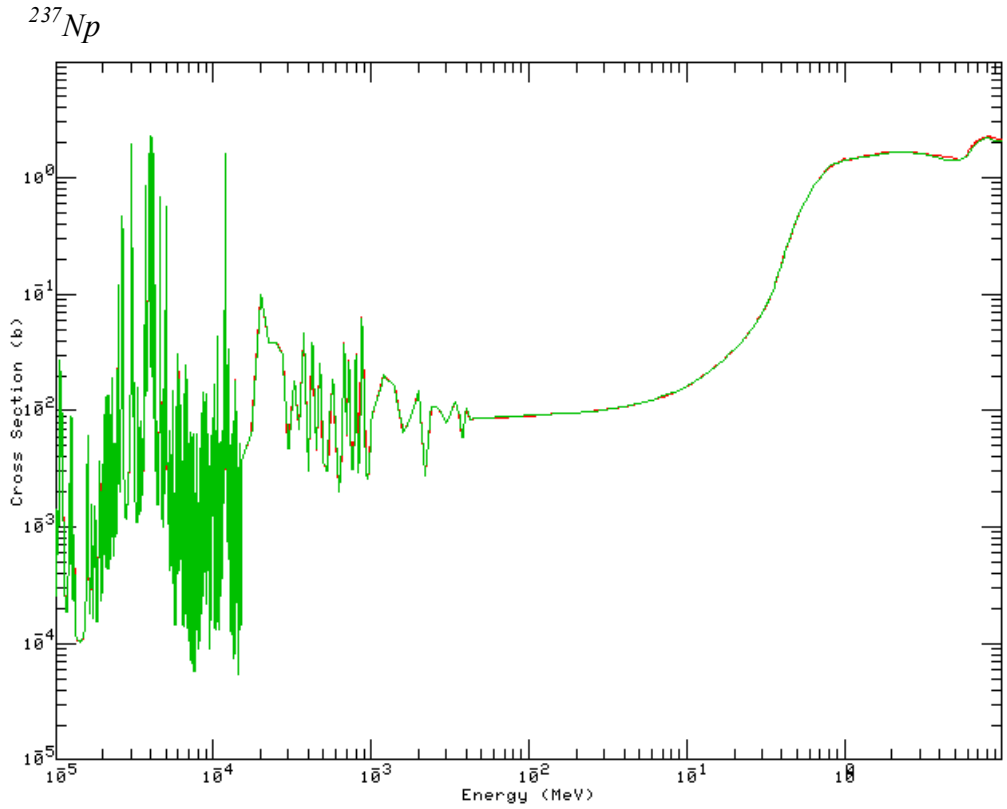

Figure 35. ^{237}Np ENDF-VI.6 fission cross section (red) and UKAEA EVAL JUL-03 (green)

^{237}Np shows little relative fission below about 100 keV (fig. 27), the approximate location of the fast fission threshold (fig. 35). Neglecting lambda values below this cut-off results in a suggested correction to the plateau cross-section value of 2.4%. It should be noted that this is very close to the margin of error in the experimental data. Overall, the nuclear data for ^{237}Np seems to be the most accurate of the actinides considered.

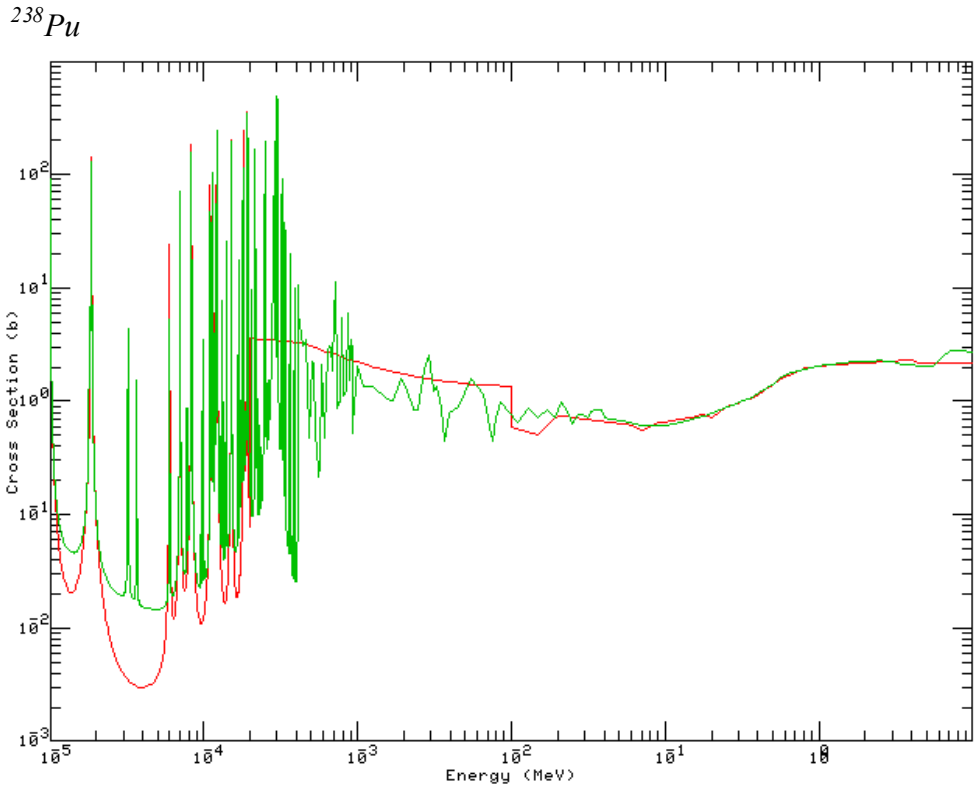

Figure 36.) ^{238}Pu ENDF-VI.6 (red) and UKAEA EVAL-JUL03 (green) fission cross section

^{238}Pu is the only minor actinide considered to have significant relative fission activity throughout much of the energy range considered (fig. 29). Additionally, the r-square values for the lambda fits for ^{238}Pu are significantly lower than those for the other actinides. Finally, the evaluated nuclear data for ^{238}Pu varies considerably, showing up to a factor of 2 to 3 difference between different data libraries in some energy regions, as seen in figure 28. However, due to the low relative fission activity in the resonance region, this analysis doesn't provide information on the energy regions with the largest differences between data sets. Unsurprisingly, the results shown in figure 28 are more difficult to draw conclusions from than for the other actinides. However, if outlying lambda sets are ignored as possible mathematical artifacts of the analysis method, a general correction factor of between 3% and 4% can be suggested for the energy range 100 eV to 1 MeV, though significantly less confidence is put in this correction factor than in those for the other actinides.

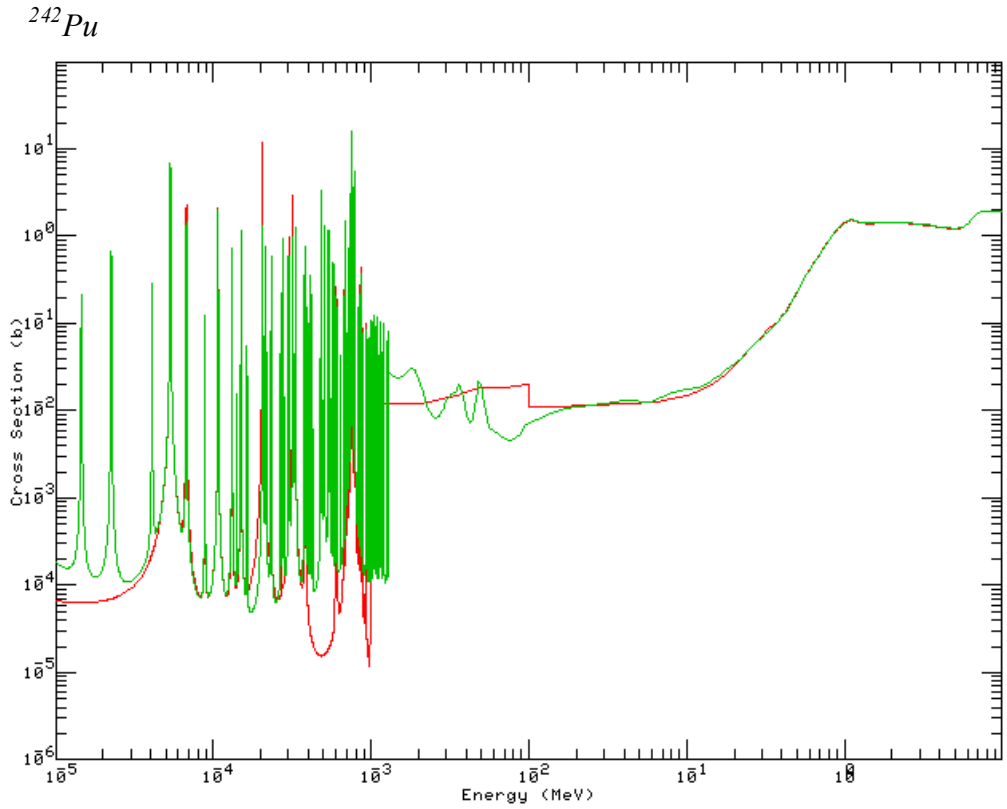

Figure 37.) ^{242}Pu ENDF-VI.6 (red) and UKAEA EVAL-JUL03 (green) fission cross section

The results for ^{242}Pu are similar to those for ^{244}Cm. Neglecting lambda values below 100 keV, where there is very limited fission activity as seen in figure 31, results in a suggested correction factor of -7% to the cross-section just above the fast fission threshold.

CONCLUSIONS

With the possibility of a closed fuel cycle being adopted in the US, the need for accurate nuclear data, particularly fission cross-section date, for the minor actinides will become more critical. The unique Japanese Fast Critical Assembly experimental facility provided fission rate data for several of the minor actinides most often considered in closed fuel cycle scenarios in 8 spectra of varying hardness. By comparing the experimental reaction rates reported to those calculated using MCNPX and the ENDF-B/VI.6 nuclear data library it was clear that some correction to the nuclear data could be made to more closely match the experimental results.

These corrections were calculated as multiplicative constants applied to a 4-group structure derived from a collapse of the 56-group experimental spectra data. Using a least squares regression, the set of lambda values most closely matching the ENDF data to the experimental results for the collapsed group structure was found. This process was then repeated several hundred times for randomly varied collapsed group structures, and the results were sorted by best fit, based on the R^2 value of the generated lambdas.

Plotting the best fit lambdas, the suggested correction to the nuclear data for most of the minor actinides was an increase or decrease of 5-10% in the plateau region above the fast fission threshold, greater than the reported experimental error. The threshold itself appeared to be located correctly in energy space, as the lambda values calculated were generally near 1.000 in the threshold region. While even the 56 group experimental reported spectra was fairly coarse, the threshold for all of the minor actinides considered was broad enough that if a change in its placement would have explained the differences between the experimental and MCNPX results, the lambda values would have indicated this.

CHAPTER 4: FISSION BLANKET DESIGN OPTIMIZATION FOR UT FISSION-FUSION HYBRID REACTOR CONCEPT

The concept of a reactor system design using both fission and fusion has been considered for over thirty years in both breeder and burner configurations. (Bethe, 1979) One of the primary difficulties in achieving an economical fusion power source is in the nature of the fusion reaction itself: whereas most of the energy liberated in a fission event is carried away by highly charged fission fragments that interact readily, the majority of fusion energy is carried away by 14.1 MeV neutrons which do not interact electromagnetically and are therefore difficult to derive energy from directly. However, if those high energy fusion neutrons could instead be used to cause fission as an external source for a subcritical fission reactor it might be possible to gain substantially more fission energy out of the combined system than fusion energy is expended.

Obviously using a large scale fusion reactor as a source of neutrons for subcritical multiplication would be a very expensive means of achieving fission. The hybrid concept is therefore typically considered for two particular applications: the breeding of excess fissile atoms in a fertile subcritical blanket, or the burning of transuranics from LWR spent fuel (Slough, 2007). Electricity generated helps to offset the system cost, but is not the only gain possible with a hybrid.

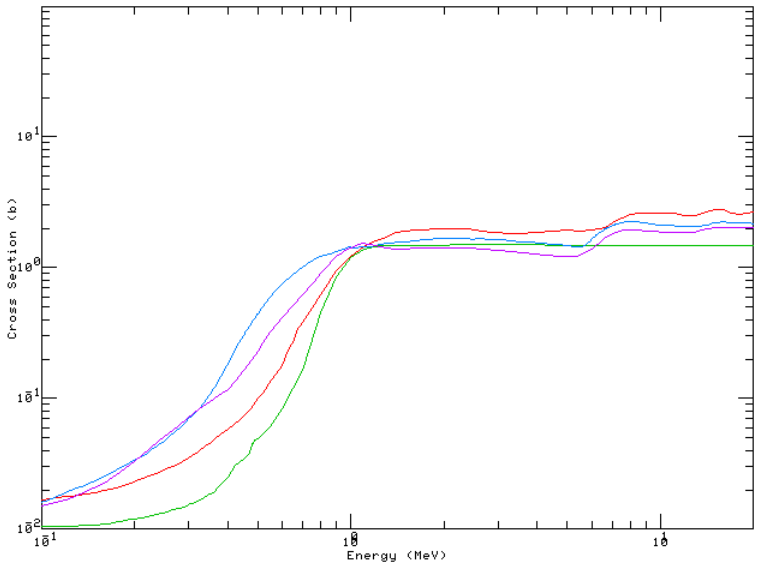

Figure 38. Fission cross section for ^{237}Np (blue), ^{242}Pu (purple), ^{241}Am (red), and ^{243}Am (green)

In a burner configuration, a fission-fusion hybrid is best suited to fissioning those minor actinides that cannot easily be disposed of in the thermal spectrum of a light water reactor or safely in a conventional fast reactor. The fission cross sections for some of these isotopes are shown above in figure 38. These isotopes are more often bred than burned in a thermal spectrum, and their low sub-fast fission threshold cross-section leads to large positive void coefficients of reactivity in fast reactors, complicating safe operation (Mukaiyama, *et al*, 1993). A hybrid design overcomes both of these problems. The fission blanket in a hybrid burner would contain little if any fertile material, minimizing any further minor actinide creation. Additionally, as it operates subcritically, a hybrid could be operated more safely than a fast reactor, provided the design had a sufficient margin to criticality in a worst case accident scenario.

However, when the concept of a fission-fusion hybrid was first explored, focus was on the potential for the system to breed excess fuel for LWRs. Designs for breeders using both ^{238}U and ^{232}Th were considered. Again, the high energy fusion neutrons drive the breeding of fissile material, especially when used in conjunction with a multiplying

material, such as the lead or the fertile actinide itself. As is seen in figure 39, the (n, Xn) reactions for these materials have thresholds between 5 and 10 MeV.

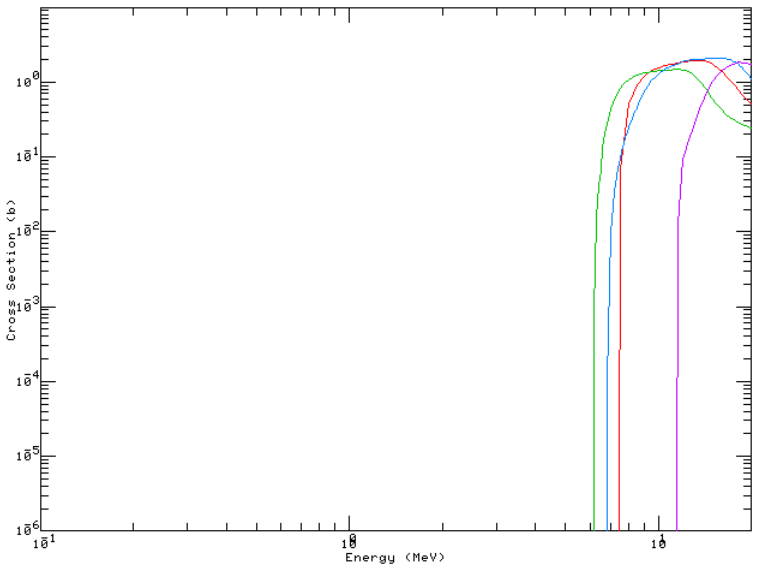

Figure 39.) Cross-section for ^{238}U (n,2n) (green), ^{207}Pb (n,2n) (blue), ^{186}W (n,2n) (red), and ^{232}Th (n,3n) (purple)

And advantage of hybrid breeder designs over fast breeders is their greater support ratio, the number of light water reactors which could be powered by the fissile material produced by one hybrid or conventional fast reactor. For conventional breeder designs the support ratio is between 1 and 2, where as for hybrids, predicted support ratios are as high as 10 (Manheimer, 1999). Therefore even though the projected cost of a hybrid may be greater than that of a conventional fast reactor, the overall capital cost required may be less.

UT'S COMPACT FUSION NEUTRON SOURCE (CFNS) HYBRID CONCEPT

While a hybrid design would have many intrinsic advantages, there are also practical and technical hurdles to overcome. For example, materials have to be capable of withstanding the high fast neutron flux of the fusion source for the duration of the system's operation. Additionally, maintenance of the internal fusion system components

is complicated by the integration of the fission blanket, reflectors, and cooling. Designed by M. Kotschenreuther, S. Mahajan, and P. Valanju of UT's Institute for Fusion Studies, and E. Schneider of the Department of Mechanical Engineering, the CFNS seeks to overcome these technical issues (Kotschenreuther, *et al,* 2009).

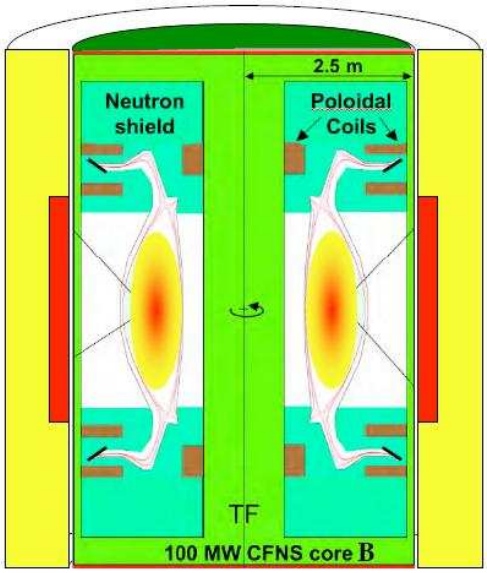

Figure 40. CFNS within fission blanket and shielding

Thanks to the Super-X diverter, the CFNS is substantially smaller than previous fusion neutron sources, capable of fitting in a large room. The advantage of this is that in the CFNS hybrid concept the fusion and fission elements are not physically connected. The CFNS would operate for a period of one to two years, at which point it could be removed and replaced by another CFNS, and then serviced. This would both decrease the length of time the equipment would be subjected to the high fast neutron flux, limiting materials concerns. Additionally, once removed, repairs to the CFNS would be much more easily completed than if they had to be performed in-situ.

Both burner and breeder configurations of the CFNS hybrid concept are considered here.

FFH-BURNER FISSION BLANKET DESIGN OPTIMIZATION

The design of the fission region of the hybrid system went through an iterative process. The materials, geometry, and placement of the fission blanket and reflectors were varied in an attempt to maximize thermal power output, while retaining a sufficiently subcritical multiplication factor in a worst case scenario. The worst case scenario for this design was an evacuation of all sodium coolant in the blanket while any sodium external to the fissioning region remained to act as a neutron reflector.

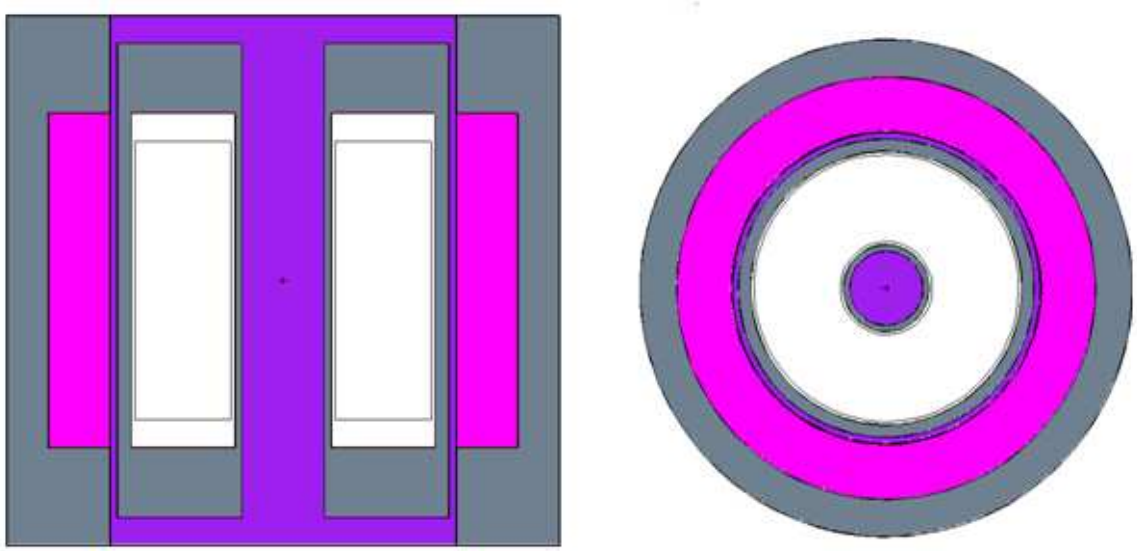

Figure 41. Initial FFH MCNP model

Initially the MCNP model used for the FFH was minimalist, with the grey regions in figure 41 representing lead reflectors, the purple aluminum, the white the fusion neutron source, and the pink region is the minor actinide laden, sodium cooled fission blanket. This first design was intended to be a loop-type: coolant channels through the outer lead and the fission blanket would remove the heat produced from fission to steam generators.

However, this initial design concept was altered in an attempt to fashion a system more obviously related to existing fast reactor designs. The new design, shown in figure 42, featured an external sodium tank containing the fissioning region with a lead intrusion

into the tank to act as a multiplier of fusion neutrons leading into the blanket. Additionally, the aluminum toroidal magnets required for the fusion source was moved to the outside of the lead shielding and slotted on the bottom to allow more fusion neutrons to reach the external tank. The level of detail in the model, while still crude, was also improved, with the Super-X diverter added along with a central core of copper.

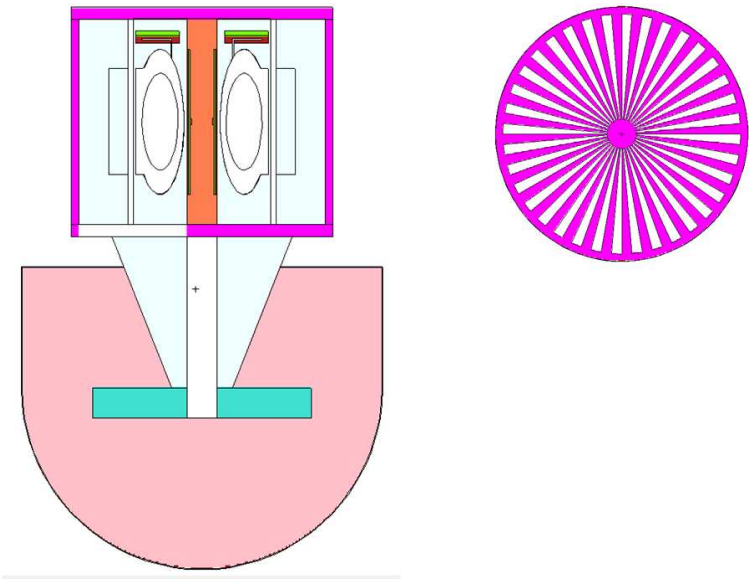

Figure 42. FFH design 2

With a pancaked fission blanket in a tank of sodium this design does share some characteristics with other existing fast reactor concepts. However, though this design has an operating multiplication factor of 0.92, within the desired range, it only generated 2.5 MWt power for the 100 MW of fusion power input to the system, several orders of magnitude short of the target output. This low power level was due to the relatively low fusion neutron flux reaching the fission region due to geometric and material attenuation.

In an attempt to increase the number of fusion neutrons reaching the fission blanket, the lead cone multiplier was hollowed out, as shown in figure 43. Void spaces were also introduced in the outer lead shielding around the fusion source to provide neutron streaming routes to the fission blanket.

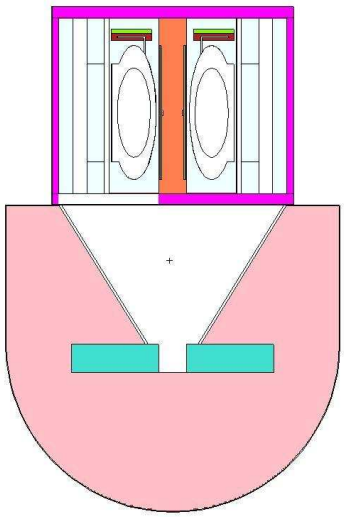

Figure 43. FFH design 3

The changes made for this design iteration resulted in a fission thermal output of 34 MW, one order of magnitude greater than the previous design, but still well short of the required energy production. Finally, to test the absolute viability of the external tank concept, the lead multiplier was removed entirely and the fission blanket was moved to the top of the tank where it would receive the maximum fusion neutron flux possible with this concept, as shown in figure 44.

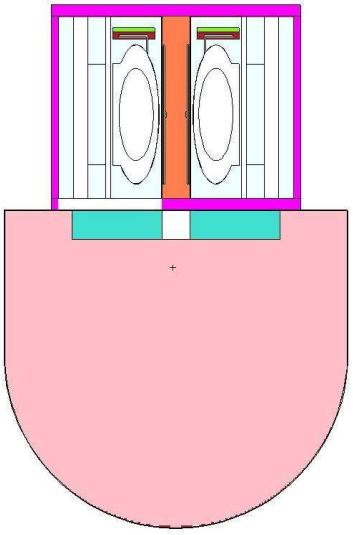

Figure 44. FFH design 4

However, even with this configuration, thermal energy output was still only 224 MWt, greater than the fusion power required, but an order of magnitude below the cut-off for economic viability. The next design move was to move the fission blanket back to its previous location in the highest flux region of the fusion source. However, the pancake shape of the blanket was retained, and the outer lead shielding was replaced by sodium coolant save for a layer adjacent to the outer aluminum, as shown in figure 45.

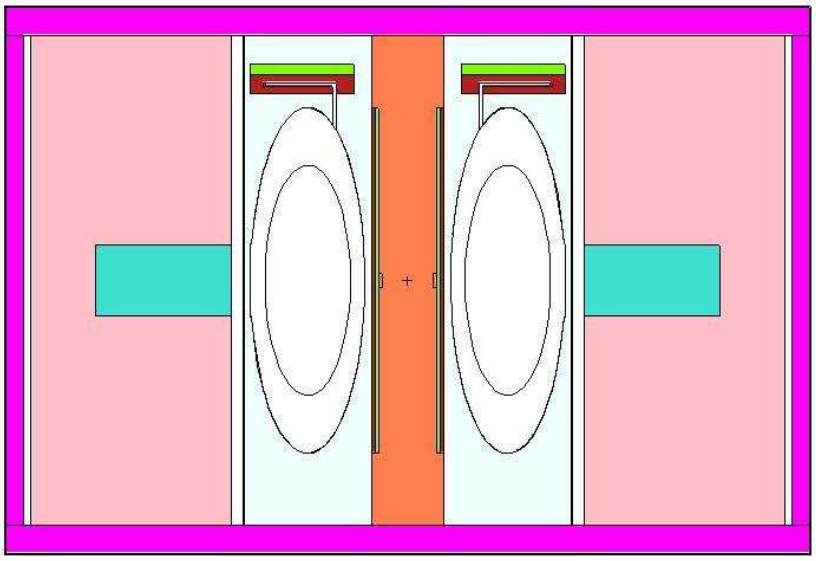

Figure 45. FFH design 5

This design resulted in fission thermal energy output of 1600 MWt, very close to the cut off for economic viability. This internal tank design was therefore selected for further modification and consideration.

The first modification was to increase the model's accuracy by adding two more Super-X diverters to mirror the two already in the design. The outer lead shielding was also replaced with tungsten to investigate its performance as a neutron multiplier as compared to lead, with additional shielding immediately horizontal to the blanket, as shown in figure 46.

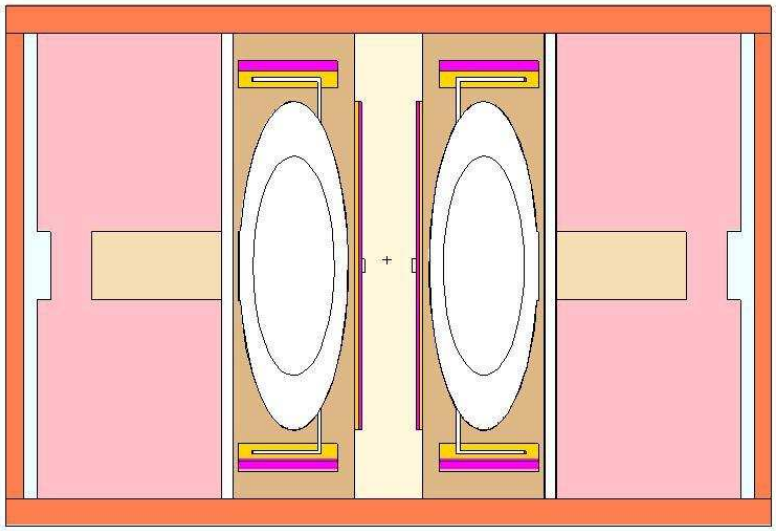

Figure 46. FFH design 6

This design resulted in a thermal output of 1500 MW and multiplication factor of 0.92, a decrease in power output primarily due to the performance of the tungsten reflector as compared to the lead, likely due to tungsten's higher absorption cross-section in the high energy region. The reflector was then changed back to lead, and the height of the fission blanket was doubled while the region volume was kept constant, as seen in figure 47.

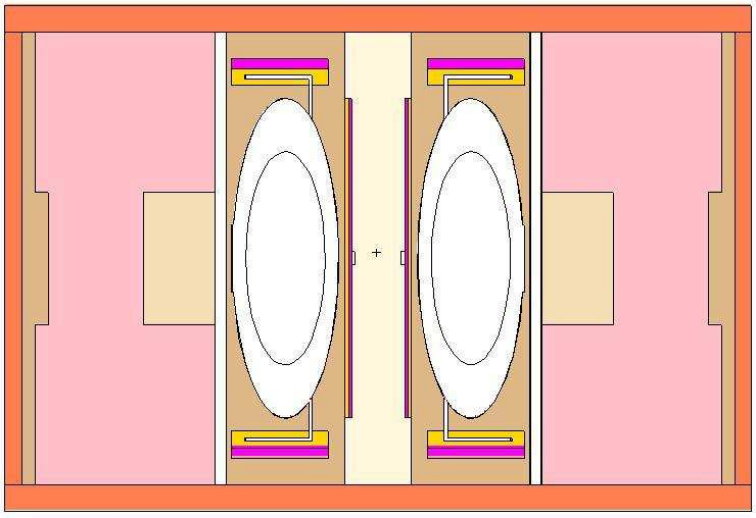

Figure 47. FFH design 7

The change in blanket geometry dramatically increased the thermal energy output to 3600 MWt from fission, above the economic breakeven point, along with a multiplication factor of 0.94. This high energy output allowed for the placement of the aluminum coils back inside the fission blanket region for the next design iteration, as seen in figure eight. The aluminum was also slotted at parallel to the fission blanket to allow for more fusion neutron streaming. Having settled on this general system concept, the final set of iterations completed was to vary the fission blanket height incrementally from 0.85 m to 3 m noting the thermal power output and operating multiplication factor as before, as well as the worst case scenario multiplication factor.

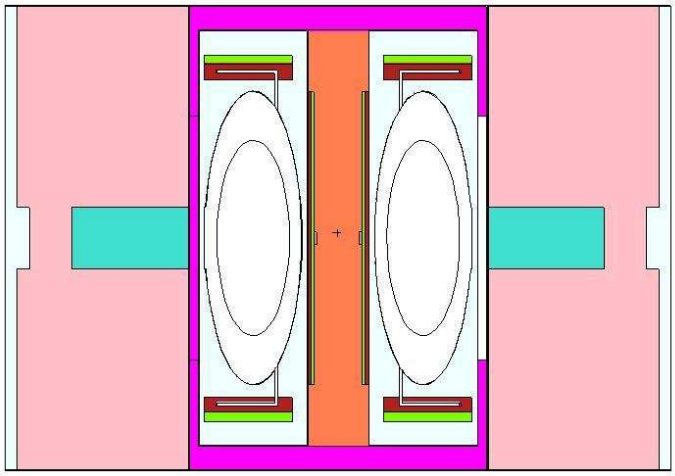

Figure 48. FFH design 8, 1 m blanket height

At a 1 m blanket height the thermal output drops to 1100 MW. The results of these design iterations are summarized in table 1, and the 0.85 m blanket and 3 m blanket configurations are shown in figures 49 and 50.

Table 7. Internal Tank Design Iterations

Blanket Height (m)	0.85	1	2	2.5	3
Operating k-eff	0.903	0.923	0.937	0.923	0.901
Accident k-eff	0.998	1.027	1.05	1.029	0.995
Thermal Output (MWt)	800	1100	2400	2300	2100

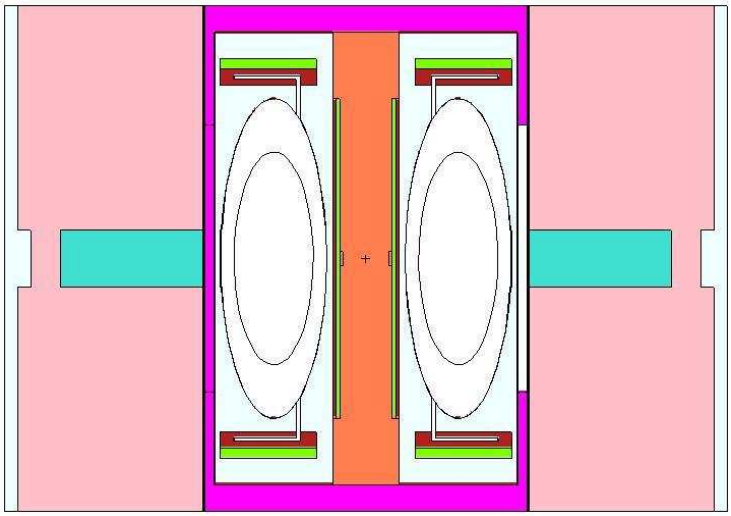

Figure 49. FFH design 8, 0.85 m blanket height

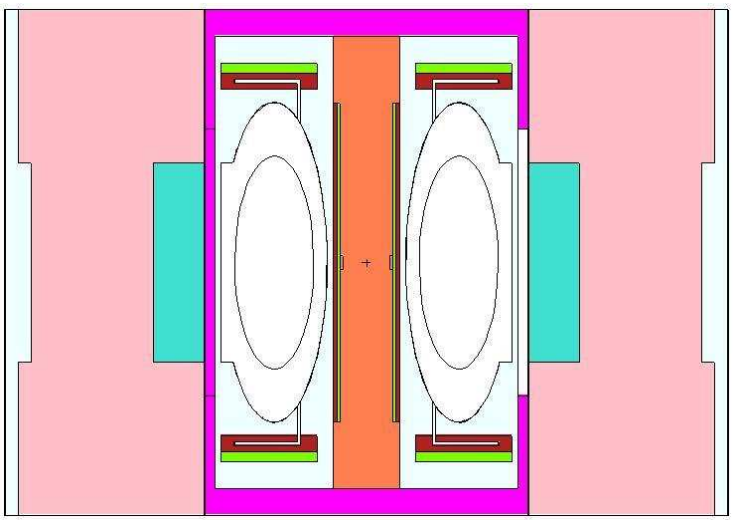

Figure 50. FFH design 8, 3 m blanket height

As can be seen in table 1, the 3 m tall blanket design is the only design to satisfy both the thermal output limit for economic viability and the subcritical multiplication in accident scenario criteria. The final burner design considered therefore returned to similar blanket geometry as was first considered in the loop-type design, though with substantial changes in the form of the internal sodium tank and decreased outer lead shielding.

FFH-THORIUM BREEDER CONCEPT

A breeder configuration of the CFNS hybrid was also considered, using ^{232}Th as the fertile material. Thorium has some advantages over ^{238}U as a breeding material; it is more prevalent in nature than uranium and the fissile isotope produced, ^{233}U, is less of a proliferation risk than ^{239}Pu due to the radiation hazard presented by the ^{232}U which is also produced. (Kang, *et al*, 2001) The breeder was modeled as seen in figure 51. The blue-gray represents the breeding blanket surrounded by aluminum magnets and a lead reflector.

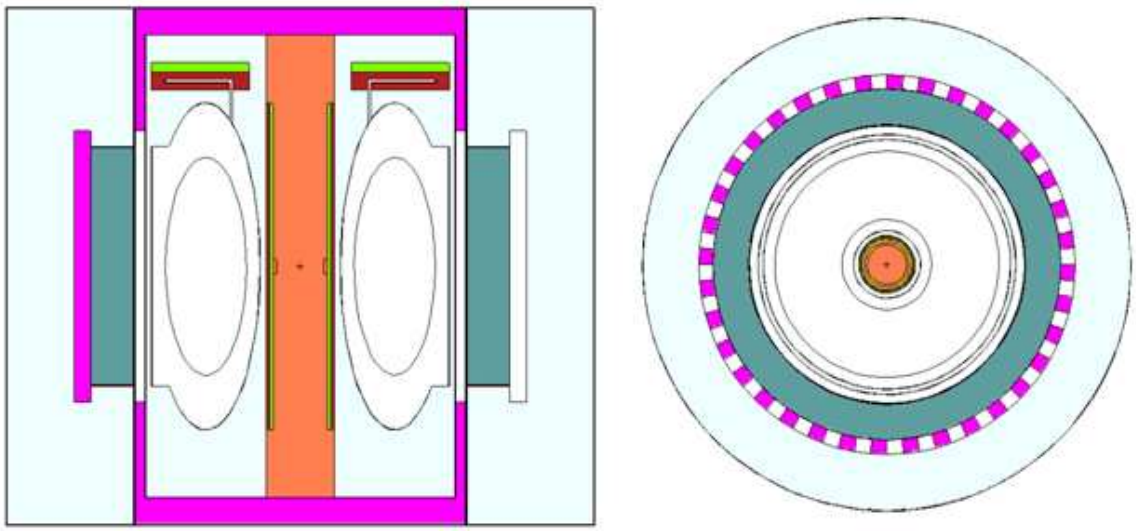

Figure 51. CFNS FFH-Thorium breeder

The breeder blanket was modeled on the design of the prismatic HTGR breeder, in which a combination of fissile and fertile micro-pebbles is embedded in graphite compacts, which in turn are placed in graphite matrix fuel elements. This design is shown in figure 52, and further characterized in table 8.

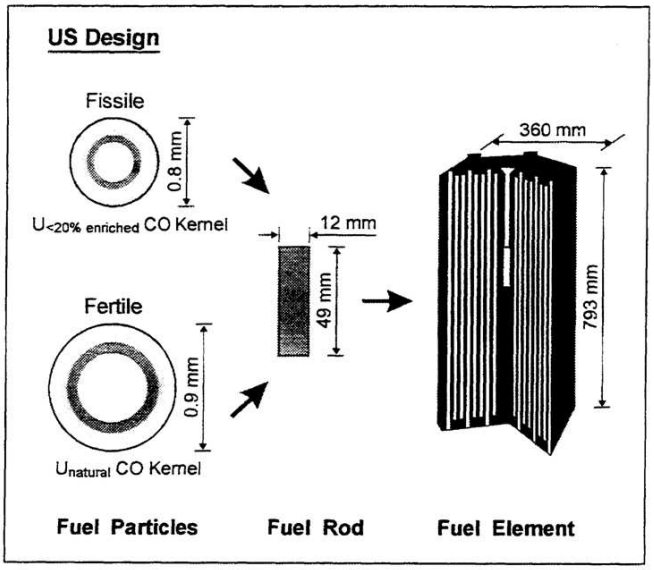

Figure 52. US reference design for fuel particles and fuel element (IAEA-TECDOC--978: Fuel performance and fission product behaviour in gas cooled reactors)

Table 8. HTGR reference TRISO fuel design (IAEA-TECDOC--978: Fuel performance and fission product behaviour in gas cooled reactors)

	FRG	US		Japan	USSR	China
Kernel		**Fissile**	**Fertile**			
Composition	UO_2	UCO	UCO	UO_2	UO_2	UO_2
Diameter [μm]	500	350	500	600	500	500
Enrichment [%]	10.6	19.9	natural	3.4 - 9.9	8.0(2)	17.0
Heavy metal loading per compact or sphere [g]	7			13.5	7.0(2)	5
Coating thickness [μm]						
Buffer	95	100	65	60	90-100	90
Inner PyC	40	35	35	30	70-80	40
Silicon carbide	35	35	35	25(1)	60	35
Outer PyC	40	40	40	45	60	40
Protective overcoating	≈ 200	-	-	≈ 200		≈ 200
Fuel element						
Type	Sphere	Block		Block	Sphere	Sphere
Graphite grade	A3-3	H-451		IG-110	30PG MPG-6	Chinese graphite
No. of coated particles per compact or sphere	≈ 11,000	≈ 6,500	≈ 3,700	≈ 13,500	13,000 - 16,000(2)	8,300

Using the above table and figure, the breeding blanket was homogenized. Next, using MCNPX, the concentration of ^{233}U necessary for a multiplication factor of 0.9 was found to be 3.0% ^{233}U. MCNPX was also used for both the 3.0% ^{233}U concentration and pure Th-232 case to calculate through reaction rate tallies the key flux weighted interaction cross-sections for ^{233}U production, as shown in figure 53. These cross-sections are summarized in tables 9 and 10.

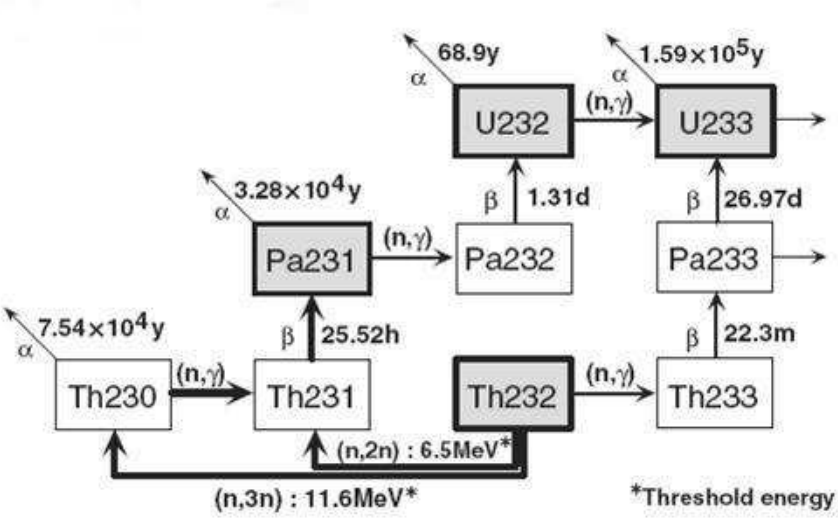

Figure 53. Production chain for ^{233}U

Table 9. ^{233}U production cross-sections for thorium only blanket

Th-232	**Calculated value**	**Thermal σ**	**U-233**	**Calculated value**	**Thermal σ**
(n,gamma)	3.746	6.50	(n,gamma)	18.854	41.00
(n,fission)	0.007	0.00	(n,fission)	181.381	469.00
ν	1.985	n/a	ν	2.523	n/a
Pa-233	**Calculated value**	**Thermal σ**	**U-234**	**Calculated value**	**Thermal σ**
(n,gamma)	38.688	34.70	(n,gamma)	50.077	87.00
(n,fission)	0.035	0.00	(n,fission)	0.241	0.01
ν	2.320	n/a	ν	2.398	n/a
U-235	**Calculated value**		**U-232 creation**	**Calculated value**	
(n,gamma)	32.842		Pa-233 (n,2n)	0.006	
(n,fission)	173.981		U-233 (n,2n)	0.002	
ν	2.466				

Table 10. U-233 production cross-sections for 3% U-233 blanket

Th-232	**Calculated value**	**Thermal σ**	**U-233**	**Calculated value**	**Thermal σ**
(n,gamma)	2.949	6.50	(n,gamma)	12.073	41.00
(n,fission)	0.008	0.00	(n,fission)	101.839	469.00
ν	1.987	n/a	ν	2.520	n/a
Pa-233	**Calculated value**	**Thermal σ**	**U-234**	**Calculated value**	**Thermal σ**
(n,gamma)	35.902	34.70	(n,gamma)	37.699	87.00
(n,fission)	0.048	0.00	(n,fission)	0.258	0.01
ν	2.321	n/a	ν	2.399	n/a
U-235	**Calculated value**		**U-232 creation**	**Calculated value**	
(n,gamma)	18.571		Pa-233 (n,2n)	0.001	
(n,fission)	86.647		U-233 (n,2n)	0.001	
ν	2.462				

Using the cross-sections from the above tables and the ORIGEN 2.2 burn-up code, two scenarios were modeled. First, for the blanket laden solely with ^{232}Th, lengthy constant flux irradiation, simulating the initial production period of ^{233}U before

multiplication due to fission. Second, for a 3% ^{233}U breeding blanket, a constant power irradiation, simulating the operating conditions of the hybrid once it has reached full power.

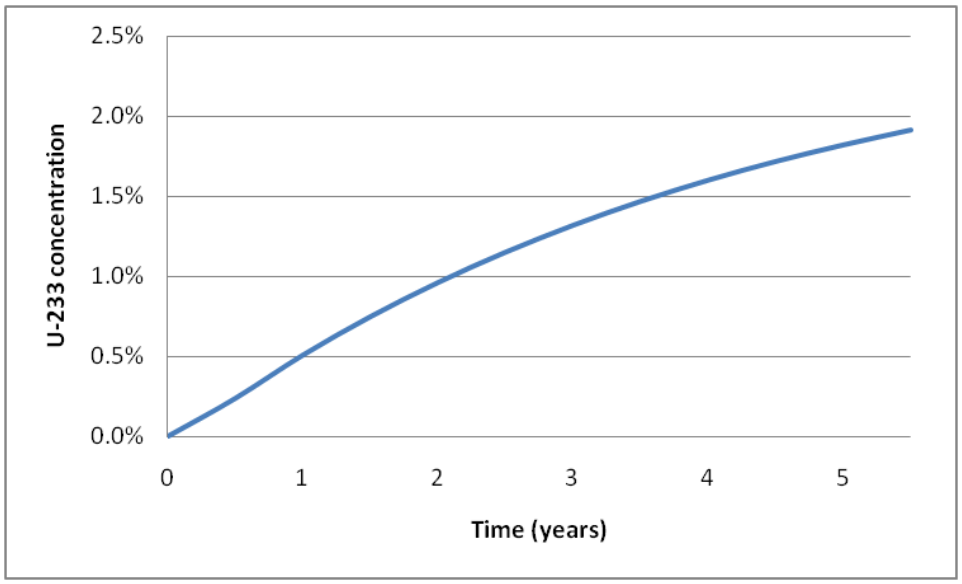

Figure 54. Fractional initial ^{233}U build up

As can be seen from figure 54, when starting from a solely fertile blanket, the required irradiation time to reach a k-eff of even 0.9 (3% ^{233}U) could be prohibitive. A Th-232 based breeding scheme using the CFNS hybrid would likely require some initial fissile material in the blanket along with the fertile ^{232}Th to boost ^{233}U production.

Analysis of the constant power irradiation case points to a similar conclusion.

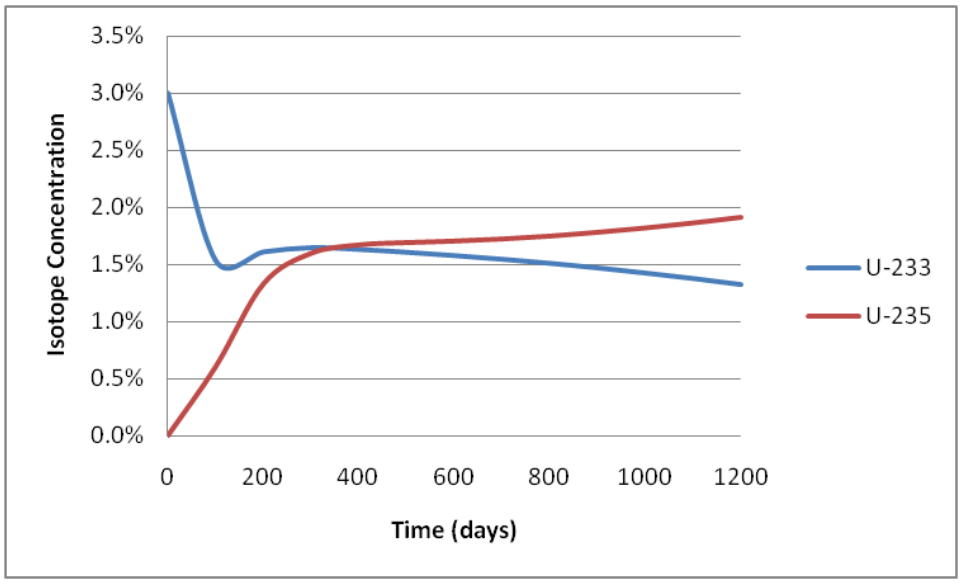

Figure 55. Fractional build up of fissile uranium at full power

As can be seen in figure 55, assuming a starting concentration of 3% ^{233}U, the total fissile material in the system drops rapidly in the first few months of irradiation as the ^{233}U burns out. Surprisingly, a good deal of this ^{233}U is replaced by ^{235}U as it is bred in to the system. However, the total mass of fissile material in the system does not increase beyond the starting value within the first several years of irradiation. From these simulations, it does not appear that a thorium based CFNS hybrid breeder would present a viable fuel production option.

CHAPTER 5: SUMMARY CONCLUSIONS

It will likely be decades before a fully closed fuel cycle exists in the United States, and in that time many remaining technical issues will need to be solved. This research sought to address aspects of three potential hurdles of an advanced fuel cycle: criticality safety of advanced reprocessing facilities, accuracy of nuclear data for the minor actinides, and design optimization of a fission-fusion hybrid for either transuranic burning or fissile material breeding.

A summary of results is as follows:

- Criticality safety standards in place for handling uranium and plutonium should be conservative by a wide margin in most cases for the minor actinide compositions found in spent nuclear fuel. Specifically, solutions of minor actinides require far greater concentrations to approach criticality than the commonly used fuel isotopes. However, when unmoderated, minor actinides may present unique criticality safety concerns due to their higher fast fission cross-sections.
- Fast fission cross-sections may in some cases be 5-10% high or low depending on the actinide. While nuclear data for some actinides, such as ^{237}Np, appears accurate to within the error of experimental data; for others, such as ^{241}Am, ^{243}Am and ^{244}Cm, the cross-section data may be incorrect. As these isotopes both dominate the long-term radiotoxicity of spent fuel and could impact design and safety of advanced burner reactors, further experimental inquiry into their interaction behavior may be warranted.
- Finally, at this stage in modeling and assuming the ability of the CFNS to provide the fusion neutron flux hoped for, the optimal placement and geometry for the fission blanket is a 3 meter tall annulus surrounding the fusion core, rather than an external pancaked shape more typically seen in conventional fast reactors. However, as a breeder of ^{233}U, the system would fail the test of economic feasibility.

These results should aid future design of reprocessing facilities and reactors which may utilize the minor actinides as fuel. In particular, the minor actinide fission cross-section correction factors produced should prove valuable as little experimental data exists for several of the species considered, and what does exist had not yet been analyzed in the manner presented here.

Further experimentation is needed to advance these projects. Benchmark criticality experiments, such as have been completed for single isotopes, for some defined reference spent fuel minor actinide composition would be useful tools in further determining safety standards for these materials. Nuclear data for the minor actinides could be further investigated at facilities such as the FCA of Japan, possibly with more finely resolved and varied spectra. In the case of the FFH, future work will have to be computational for many more years, though plenty of computational design optimization remains to be done.

Appendices

APPENDIX A: SPENT AND EQUILIBRIUM FUEL COMPOSITIONS

	25 GWd/t	*45 GWD/t*	*65 GWD/t*
Np237	3.71734%	6.17132%	7.55033%
Pu238	0.65652%	2.21371%	4.22633%
Pu239	62.63893%	45.99561%	37.36594%
Pu240	22.32547%	23.73604%	20.95290%
Pu241	8.68310%	13.59546%	13.37819%
Pu242	1.57148%	5.90430%	9.95335%
Am241	0.17793%	0.42885%	0.46789%
Am242m	0.00325%	0.00964%	0.01147%
Am243	0.16494%	1.33674%	3.61984%
Cm242	0.03766%	0.16263%	0.24661%
Cm244	0.02338%	0.44571%	2.22715%

Spent fuel TRU isotopic compositions

Np237	2.03796%
Pu236	0.00002%
Pu238	4.32567%
Pu239	36.66333%
Pu240	33.36663%
Pu241	5.20479%
Pu242	8.73127%
Am241	3.32667%
Am242m	0.25574%
Am243	3.01698%
Cm242	0.02997%
Cm243	0.01698%
Cm244	2.12787%
Cm245	0.57742%
Cm246	0.31868%

Equilibrium TRU isotopic composition

APPENDIX B: COMPLETE MINOR ACTINIDE INITIAL LAMBDA CORRECTIONS

Pu-238: ENDF-B/VI.6

λ_4	0.9820
λ_3	0.9831
λ_2	1.0578
λ_1	0.9979

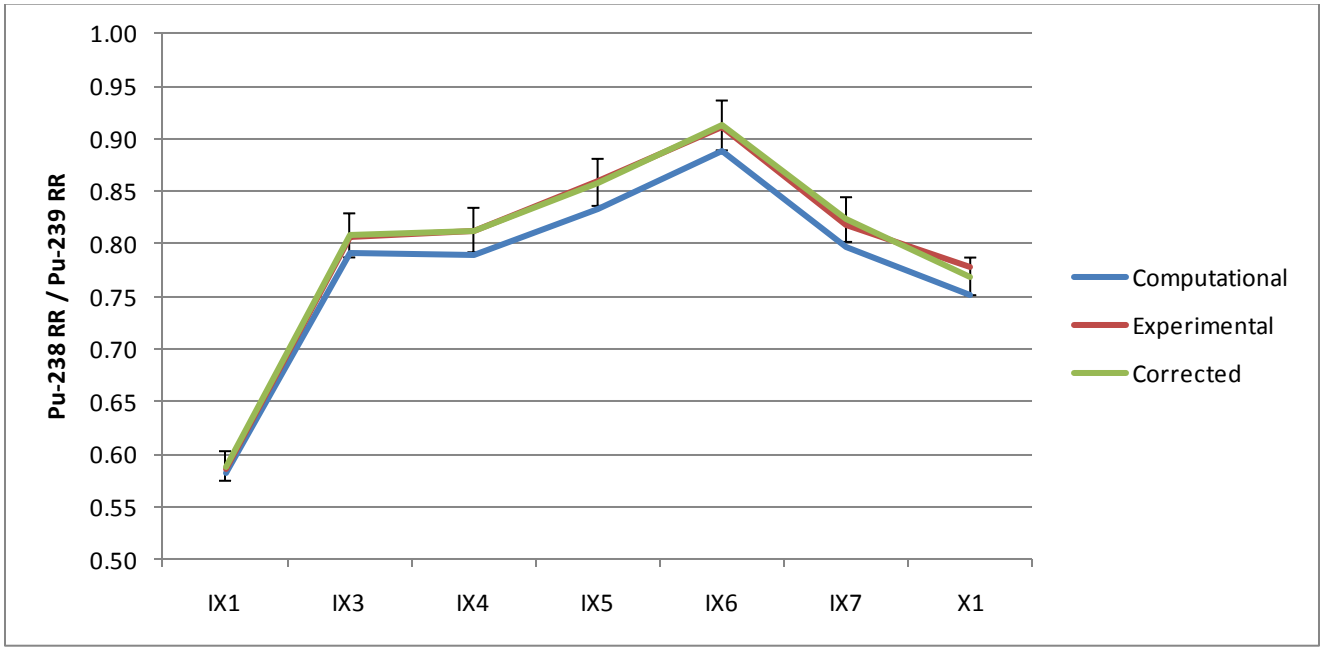

Pu-242: ENDF-B/VI.6

λ_4	0.9999
λ_3	0.9994
λ_2	0.9679
λ_1	0.9166

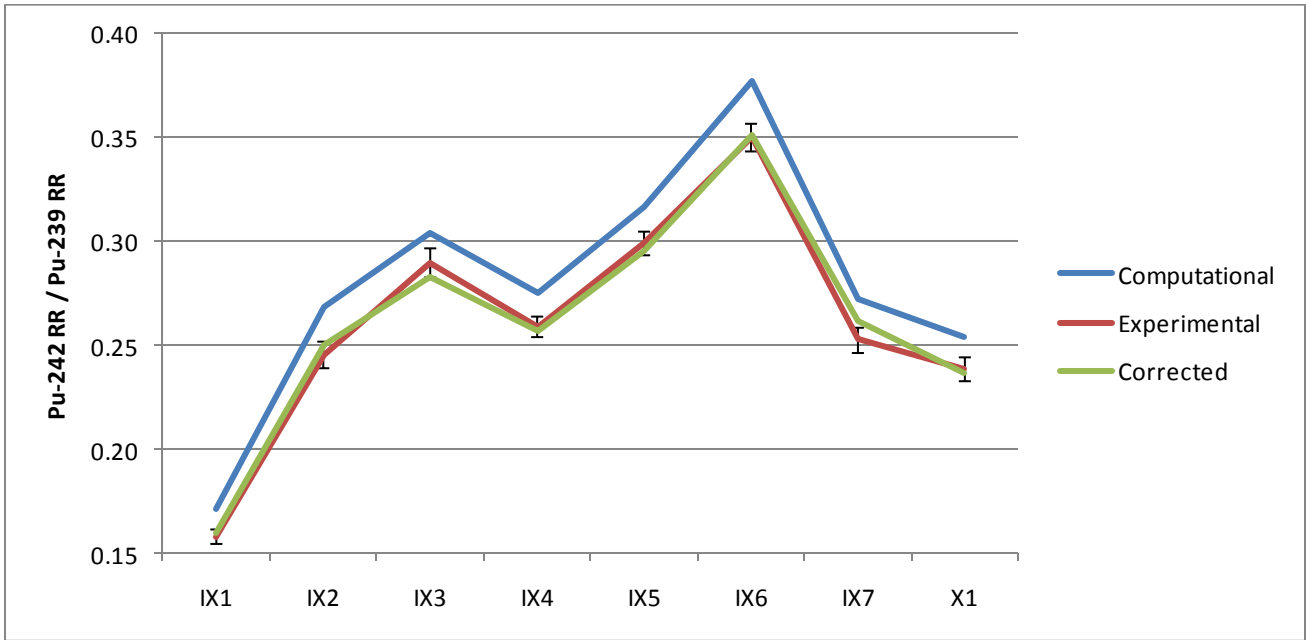

Am-241:ENDF-B/VI.6

λ_4	1.0000
λ_3	1.0004
λ_2	1.0106
λ_1	1.0447

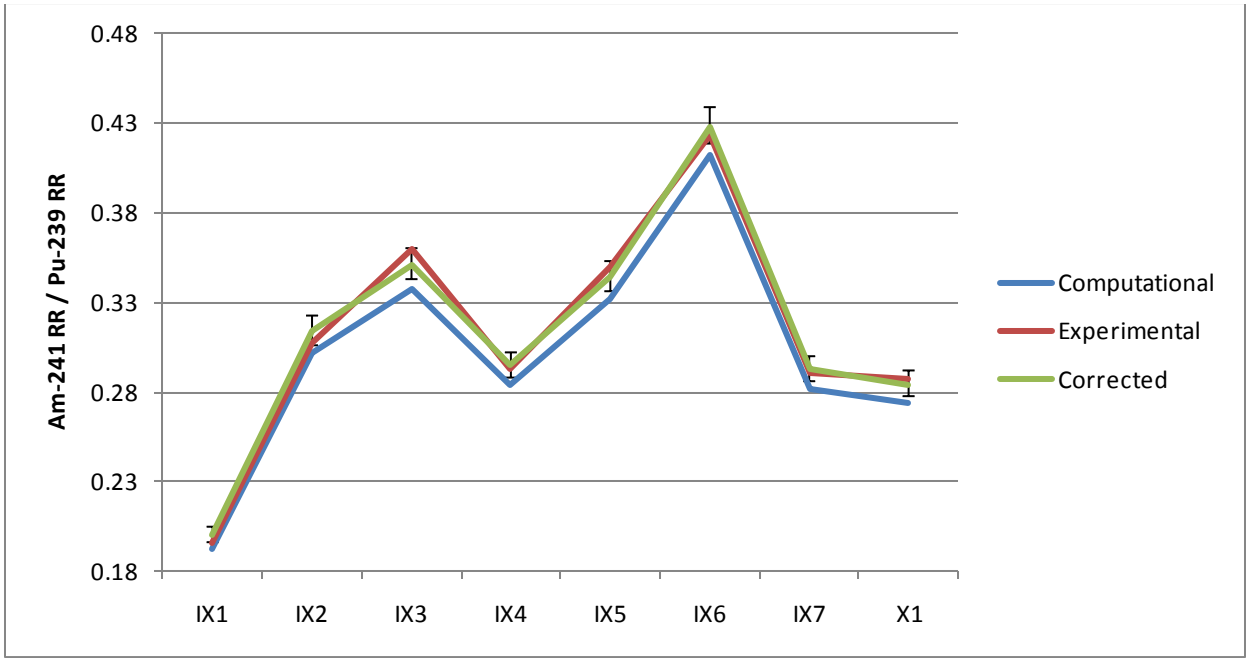

Am-241 : ENDF-B/V

λ_4	0.9999
λ_3	0.9996
λ_2	0.9936
λ_1	0.9700

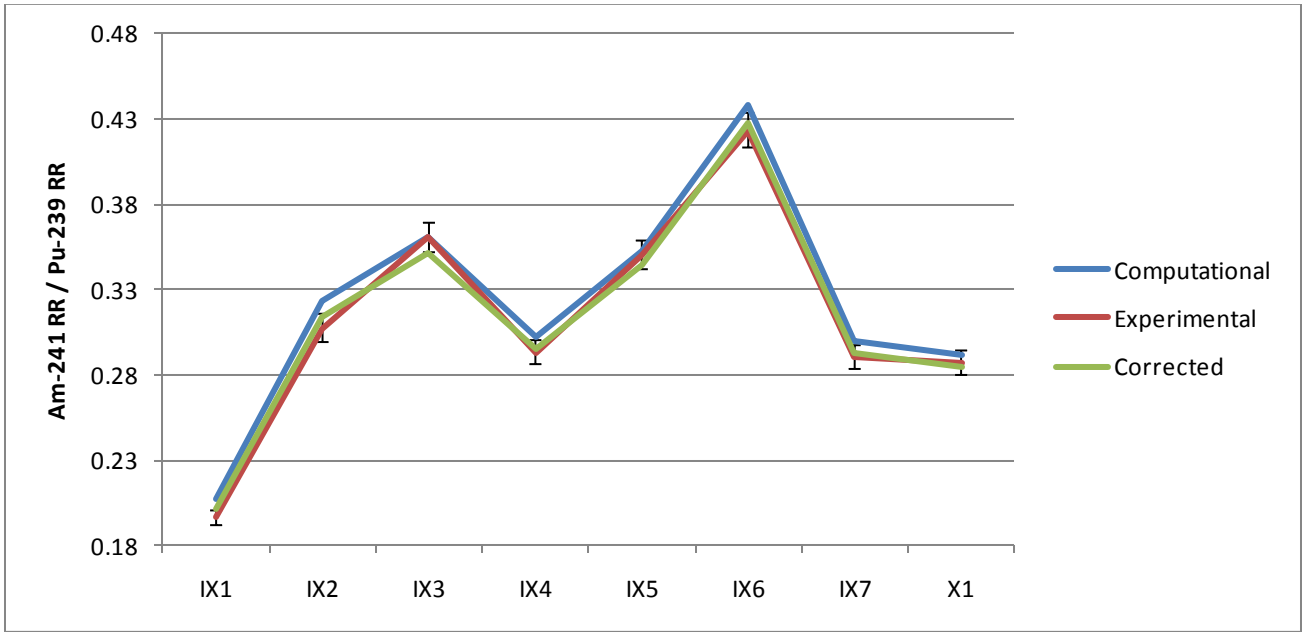

Cm-244: ENDF-B/VI.6

λ_4	1.0000
λ_3	0.9989
λ_2	0.9642
λ_1	0.9342

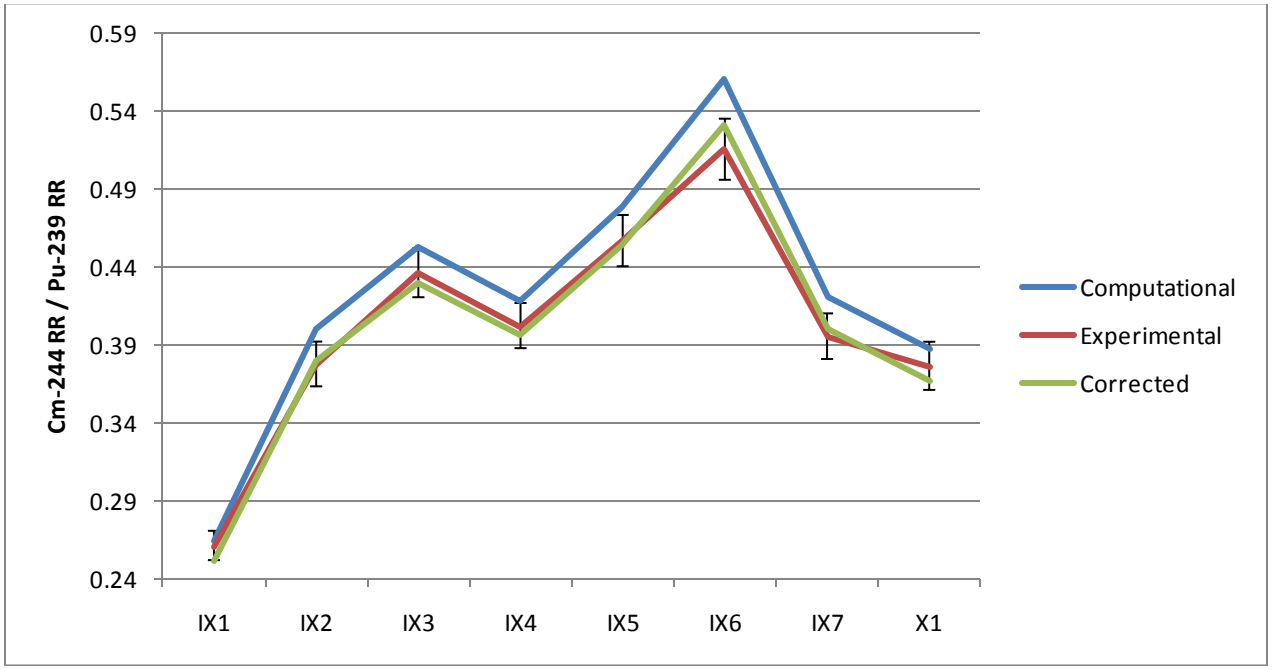

References

H. BETHE, "The Fusion Hybrid," Physics Today, The American Institute of Physics, May 1979

International Atomic Energy Agency, "TECDOC--978: Fuel performance and fission product behaviour in gas cooled reactors," 1997

Japan Atomic Energy Agency, Reactor Physic Group, Fast Critical Facility overview, available at http://rpg.jaea.go.jp/oldHP/index.htm

J. KANG, F. VON HIPPEL, "U-232 and the Proliferation Resistance of U-233 Spent Fuel," Science & Global Security, Vol. 9, Taylor and Francis, 2001

Korea Atomic Energy Research Institute, Cross-Section Plotter, available at http://atom.kaeri.re.kr/

M. KOTSCHENREUTHER *et al.*, "Fission-Fusion Hybrid to Destroy Nuclear Waste: From a Challenge to an Opportunity," The University of Texas at Austin, April 2009

J. LAIDLER, *et al.*, "Chemical Partitioning Technologies for an ATW System," Progress in Nuclear Energy, 2001

W. MANHEIMER, "Can Fusion Research be Revitalized by Embracing a Fission-Fusion Hybrid Reactor?", Fusion Summer Study, July 1999

T. MARTINEZ, "Accelerator Transmutation of Waste," Science for the 21st Century, Los Alamos National Laboratory Public Affairs Office, 2000

A. MENGONI, *et al.*, "International Efforts to Measure, Model, and Evaluate Nuclear Data for the Minor Actinides," Proc. International Conference on the Physics of Reactors, 2008

T. MUKAIYAMA, *et al.*, "Minor Actinide Burner Reactor and Influence of Transmutation on Fuel Cycle Facilities," Japan Atomic Energy Agency, IAEA-TECDOC--783: Safety and environmental aspects of partitioning and transmutation of actinides and fission products, 1993

Nuclear Energy Institute, "Nuclear Waste Disposal for the Future: The Potential of Reprocessing and Recycling," available at http://www.nei.org/filefolder/whitepaper_reprocessingandrecycling_0306.pdf, 2006

S. OKAJIMA *et al.*, "Benchmark test for TRU nuclear data by analysis of central fission rate ratios measured at FCA cores," Proc. International Conference on the Physics of Reactors, Japan Atomic Energy Agency, 2008

S. OKAJIMA *et al.*, "Benchmark test for JENDL 3.3 Library by Analyses of a Series of Experiments at the Fast Critical Assembly (FCA) of JAERI," Proc. International Conference on the Physics of Reactors, Japan Atomic Energy Agency, 2008

ORIGEN 2.2: "Isotope Generation and Depletion Code Matrix Exponential Method," Oak Ridge National Laboratory, Radiation Safety Information Computational Center, August 1996

D. PELOWITZ, "MCNPX^{TM} User's Manual, version 2.5.0," LA-CP-05-0369, April 2005

B. POHL *et al.*, "Criticality Experiments with Mixed Plutonium and Uranium Nitrate Solution at a Plutonium Fraction of 0.2 and 0.5 in Large Cylindrical Geometry,", NEA/NSC/DOC(95)03/VI, Vol. VI, LLNL, September 2000

T. SASA, "Partitioning and Transmutation Studies at JAEA," International Workshop for Asian Nuclear Prospect, J-PARC center, JAEA, 2008

J. SLOUGH, "Suitability of Small Scale Linear Systems for a Fission-Fusion Reactor, Breeder, and Waste Transmutation," Journal of Fusion Energy, 2008

W. STANBRO, "Production and Measurement of Minor Actinides in the Commercial Fuel Cycle," Los Alamos 13248-MS, March 1997

Vita

Christopher Ainslie van der Hoeven was born in Manhattan, KS, and later moved to Raleigh, NC. After completing his work at North Raleigh Christian Academy, Raleigh, NC in 2003, he entered the Nuclear Engineering program at Texas A&M University in College Station as a National Merit Scholar. He received the degree of Bachelor of Science from Texas A&M University in December, 2007. In January, 2008 he entered the Nuclear and Radiation Engineering graduate program at The University of Texas, where he is currently working towards his Ph.D.

E-mail: cvanderh@mail.utexas.edu

This thesis was typed by the author.